

Re-assessing ImageNet: How aligned is its single-label assumption with its multi-label nature?

Esla Timothy Anzaku^{1,2}, Seyed Amir Mousavi^{1,2}, Arnout Van Messem³, Wesley De Neve^{1,2}

¹Ghent University, Belgium

²Ghent University Global Campus, South Korea

³University of Liège, Belgium

Abstract

ImageNet, an influential dataset in computer vision, is traditionally evaluated using single-label classification, which assumes that an image can be adequately described by a single concept or label. However, this approach may not fully capture the complex semantics within the images available in ImageNet, potentially hindering the development of models that effectively learn these intricacies. This study critically examines the prevalent single-label benchmarking approach and advocates for a shift to multi-label benchmarking for ImageNet. This shift would enable a more comprehensive assessment of the capabilities of deep neural network (DNN) models. We analyze the effectiveness of pre-trained state-of-the-art DNNs on ImageNet and one of its variants, ImageNetV2. Studies in the literature have reported unexpected accuracy drops of 11% to 14% on ImageNetV2. Our findings show that these reported declines are largely attributable to a characteristic of the dataset that has not received sufficient attention – the proportion of images with multiple labels. Taking this characteristic into account, the results of our experiments provide evidence that there is no substantial degradation in effectiveness on ImageNetV2. Furthermore, we acknowledge that ImageNet pre-trained models exhibit some capability at capturing the multi-label nature of the dataset even though they were trained under the single-label assumption. Consequently, we propose a new evaluation approach to augment existing approaches that assess this capability. Our findings highlight the importance of considering the multi-label nature of the ImageNet dataset during benchmarking. Failing to do so could lead to incorrect conclusions regarding the effectiveness of DNNs and divert research efforts from addressing other substantial challenges related to the reliability and robustness of these models.

1. Introduction

The ImageNet dataset [7, 19] continues to be a key benchmark to evaluate the progress of deep neural networks (DNN) in computer vision. It comprises two main subsets: ImageNet-1K, a widely used dataset with 1,000 classes and more than 1 million images, mainly used for single-label classification tasks; and ImageNet-22K, an extended dataset containing around 22,000 classes and over 14 million images, which captures a much wider range of object categories. ImageNet-1K plays a central role in benchmarking both classical and state-of-the-art (SOTA) architectures, such as ResNet [11], Vision Transformers [8], and ConvNext [15]. Beyond supervised learning, ImageNet-1K was proven valuable in self-supervised learning by facilitating the assessment of models that learn effective visual representations without labeled data [4, 10, 12, 16]. Moreover, it has become integral in the evaluation of vision language models, where zero-shot performance in ImageNet-1K classification is often used as a metric to measure transfer learning capabilities and visual recognition skills [5, 17, 23]. However, as model effectiveness on ImageNet-1K saturates, its shortcomings become more apparent. One critical issue is that many images in the dataset can belong to multiple valid categories, yet the dataset imposes a single-label constraint, which has been identified as a fundamental limitation [3, 20]. This discrepancy between the inherent multi-label nature of real-world data and the single-label approach used for ImageNet-1K is understudied, despite its potential to impact the evaluation of model robustness and generalization. Addressing this issue is vital, especially as ImageNet-1K continues to play an important role in evaluating cutting-edge models in self-supervised and zero-shot learning contexts.

In this study, we revisit the ImageNet-1K benchmark to examine the discrepancy between the conventional single-label approach and the multi-label nature of the dataset. We analyze the limitations of the single-label evaluation approach and demonstrate the advantages of adopting a multi-

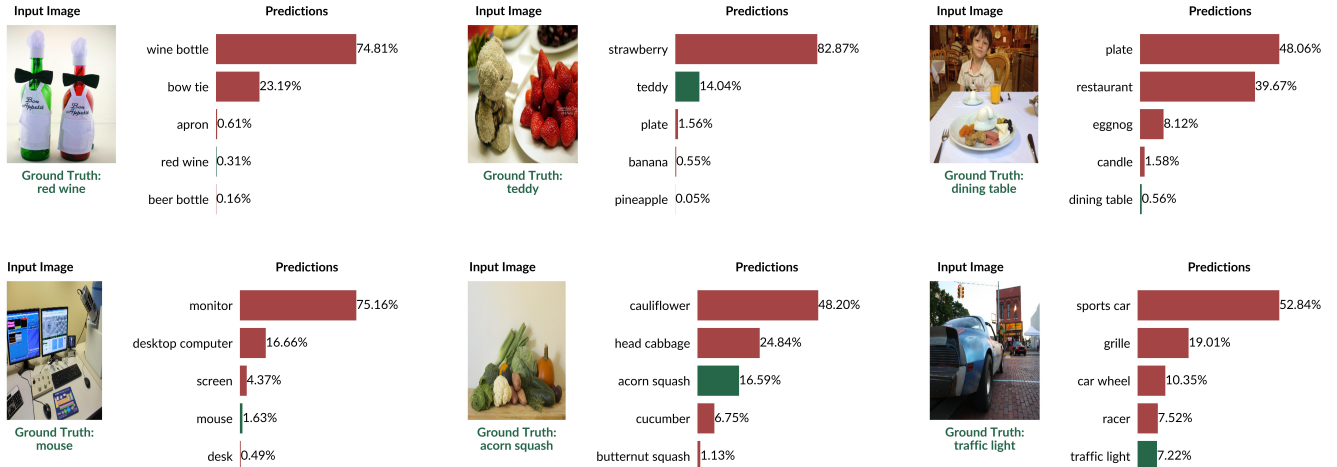


Figure 1. Examples from ImageNetV2 showing the top-5 predictions of a pre-trained DNN model. The percentages indicate the softmax scores of each top-5 prediction. Ground-truth labels and correct predictions are highlighted in green, while incorrect predictions are in red. While the model predictions capture the complexities of the images, evaluating the model based solely on the provided single ground-truth labels may obscure the multi-label nature of some images and underestimate the effectiveness of a model.

label perspective in assessing model effectiveness. Our investigation focuses on the reported degradation in effectiveness of DNNs on replicate test datasets, such as ImageNetV2 [18], which was created using the same methodology as the original ImageNet-1K dataset. For the remainder of this paper, we will refer to the validation set of the ImageNet-1K dataset as *ImageNetV1*. Despite being carefully created following the same protocols as ImageNetV1, the accuracy of pre-trained ImageNet models on ImageNetV2 has been reported to drop between 11% and 14%, and overfitting was ruled out as the likely factor [18]. In another work, statistical bias in the replication process has been suggested as a possible explanation [27]. However, the role of the single-label assumption in this degradation in effectiveness remains understudied.

We aim to answer the question: *Are we inadvertently attributing a degradation in effectiveness to model shortcomings or benign dataset characteristics, while overlooking implicit assumptions embedded in datasets and the limitations of our evaluation methodologies?* To illustrate the potential of DNNs in capturing the multi-label nature of images, we present, in Figure 1, the top-5 predictions of a selected number of ImageNetV2 images. The predictions were generated using a highly effective model pre-trained on ImageNet [31, 33]. Under the top-1 accuracy metric, these examples would be considered incorrect predictions. However, upon closer examination, we can observe the capability of the model in discerning the multi-label nature of the images, highlighting the need for a more comprehensive evaluation approach.

We propose the adoption of a multi-label evaluation framework for model benchmarking on ImageNet-1K and

its variants. This framework seeks to provide a more robust assessment of the ability of SOTA DNNs to capture complex label distributions within the ImageNet-1K dataset. It ensures that model effectiveness is evaluated in a way that more comprehensively reflects the inherent multi-label complexity of the data. Although the creation of a comprehensive multi-label dataset is resource-intensive, we contend that, at a minimum, the test sets must closely represent the inherent multi-label nature of the dataset. This approach is fundamental to developing a deeper understanding of the inherent strengths and limitations of DNNs, aiming to enhance their robustness and reliability. In particular, overcoming the limitations of the single-label assumption is essential to fully unlock the potential of DNNs for analyzing and engaging complex visual data.

In line with our commitment to improve the benchmarking of DNNs using ImageNet-1K and its variants, we summarize the contributions of this paper in the following.

- **Variation in Multi-Label Proportions between ImageNetV1 and ImageNetV2:** We identify a previously unrecognized variation in the proportion of multi-label images between ImageNetV1 and ImageNetV2, with ImageNetV2 containing a notably higher proportion of images with multiple valid labels. This difference in label structure is a key factor that contributes to model performance discrepancies in ImageNetV2.
- **Consequences of Ignoring Multi-Label Characteristics in ImageNet Benchmarks:** We analyze the impact of disregarding the multi-label characteristics in ImageNetV1 and ImageNetV2 benchmarks. Our results show that the single-label assumption, coupled with top-1 accuracy, penalizes models for selecting valid alterna-

tive labels, leading to an overstated performance drop on ImageNetV2. Accounting for multi-label attributes reveals that model effectiveness on ImageNetV2 remains more consistent with ImageNetV1 than previously reported in [18].

- **The Multi-Label Prediction Capability of Pre-Trained Models:** Although the ReaL accuracy [3] provides insights into the multi-label prediction capabilities (MLPC) of DNNs pre-trained on ImageNet, it has a limitation. Only the top prediction is considered without accounting for other valid predictions. This limitation could lead to a reduced ability to differentiate between the MLPC of different models. Considering that there is no established approach to infer multi-label prediction from multi-class classification models for evaluation purposes, in Section 3.1, we introduce the use of the top- k predictions, where k varies depending on the number of available ground truth labels per image.
- **Patch-Based Multi-Label Dataset Generation:** Influential datasets in image recognition, such as ImageNet-1K, provide object detection annotations for certain subsets, though these are rarely used for benchmarking. Our methodology re-purposes these annotations to create additional test datasets for rigorously assessing the MLPC of pre-trained multi-class classification models, as described in Section 3.2.

2. Related Work

Identified Multi-label Issues with ImageNet Beyer et al. [3] highlighted a critical issue in ImageNetV1: the misalignment between the single-label assumption for ImageNet and its inherently multi-label nature. To address this, they introduced the ReaL (Reassessed Labels) accuracy, which accommodates multiple valid labels per image, providing a more accurate evaluation of model effectiveness. In a related study, Shankar et al. [20] employed human annotators to meticulously re-label subsets of the ImageNetV1 and ImageNetV2 datasets. Their analysis demonstrated that approximately 20% of the images in ImageNetV1 contain more than one valid label. As a result, they concluded that top-1 accuracy underestimates model effectiveness in multi-label contexts, while top-5 accuracy tends to overestimate it. Building on these insights into the multi-label nature of ImageNet, Tsipras et al. [27] identified that over 20% of ImageNet images contain multiple objects, despite being annotated with a single ground-truth label. This misalignment leads to biases in model evaluation, as top-1 accuracy penalizes models for predicting valid, but unannotated, labels. Their findings highlight the need for benchmarks that better reflect the complexity of real-world tasks. To assess the extent of multi-label presence in ImageNet replicate datasets, Anzaku et al. [2] re-labeled the ImageNetV2 dataset and found that approximately 48% of the images contain more

than one valid label. Our work builds on these findings and further explores the impact of varying proportions of multi-label images between ImageNetV1 and ImageNetV2 on the reported accuracy degradation of ImageNetV2, which is detailed in the following paragraph.

Accuracy Degradation of Pre-trained ImageNet Models on ImageNetV2

Several studies have used ImageNetV2 for benchmarking and have consistently reported a degradation of effectiveness compared to ImageNetV1. Recht et al. [18], who created the ImageNetV2 dataset, evaluated a range of pre-trained ImageNet models on it and observed an accuracy drop of 11% to 14%. They attributed this decline to models struggling with “slightly harder” images, indicating potential challenges in generalization. In a separate analysis, Engstrom et al. [9] explored potential sources of bias in the ImageNetV2 dataset, concluding that statistical bias in the model replication process might account for part of the gap in effectiveness. After adjusting for this bias, they found that only 3.6% of the accuracy degradation remained unexplained. Similarly, Anzaku et al. [1] used uncertainty estimates from DNN models in their assessment and suggested that the top-1 accuracy metric alone, without leveraging the uncertainty from the models, may overestimate the extent of the observed degradation. Although these studies provide valuable information on the causes of the drop in effectiveness, none have conclusively linked the degradation to a specific modeling issue or a property of the dataset.

ImageNet Benchmark Underestimating Effectiveness

Recent studies indicate that the effectiveness of convolutional networks in ImageNet benchmarks may be vastly underestimated. Stock and Cisse [21] found that when human evaluators reviewed model predictions, the top-1 error rate of a ResNet-101 in the ImageNet validation set decreased from 22.69% to 9.47%, and the top-5 error dropped from 6.44% to 1.94%. This work highlights the limitations of current evaluation metrics and suggests that traditional accuracy benchmarks might not fully capture the capabilities of deep neural networks. Building on this, Vasudevan et al. [28] conducted a careful expert multi-label re-evaluation and categorization of the remaining mistakes made by top models on multi-label subsets of ImageNetV1 and ImageNetV2. They found that nearly half of these errors were not actual errors but valid predictions that were penalized due to the single-label assumption, label noise, and fine-grained object confusion. By re-annotating subsets of the datasets to include multiple valid labels and correct erroneous ones, the models achieved up to 97.9% multi-label accuracy, substantially reducing the error rate and providing insights into the long-tail of errors. Similarly, Taesiri et al. [24] demonstrated that pre-trained ImageNet mod-

els could achieve up to 98.91% accuracy on ImageNet by strategically zooming in the most informative regions of an image. By adjusting the framing to focus on key discriminative features, models were able to substantially improve their classification effectiveness, while disregarding less relevant background details. This approach highlights the importance of framing and scale in image classification, suggesting that much of the observed gaps in effectiveness may be due to sub-optimal image focus rather than inherent model deficiencies.

Single Positive Multi-label Learning Given the evidence of the multi-label nature of the ImageNet dataset and its replicates, a straightforward solution to this issue is adopting multi-label classification. However, for large datasets of the scale of the ImageNet dataset, creating high-quality multi-label annotations for training is prohibitively expensive. A promising research approach introduced in the literature is the Single Positive Multi-label Learning (SPML) approach [6], which assumes that for each image, only one positive label is provided, while multiple unannotated but valid labels may exist. Verelst et al. [29] utilized this approach and demonstrated its viability for large vision datasets including the ImageNet dataset. By leveraging the known relationships between classes and the shared structure within the data, SPML methods can propagate single positive labels to infer other relevant labels during training. This substantially reduces the labeling burden while allowing models to generalize in multi-label scenarios.

3. Methodology

The methodology we introduce in this paper can be applied to a wide range of multi-class classification computer vision datasets, where the datasets are arguably multi-label in nature. However, we focus on the ImageNet benchmark due to its pivotal role in the progress of deep learning for computer vision. Although multi-label versions of the labels for ImageNetV1 and ImageNetV2 exist, we are not aware of established methods to derive multi-label predictions from ImageNet pre-trained models. To fill this gap, we propose a baseline approach in Section 3.1 for deriving multi-label prediction sets from pre-trained models for evaluation purposes. Furthermore, to augment the multi-label annotations available for the assessment of DNNs on the ImageNetV1 and ImageNetV2 datasets, we introduce a method for dynamically generating multi-label datasets from publicly available annotations for the ImageNet Object Localization Challenge ¹ in Section 3.2.

¹<https://www.kaggle.com/c/imagenet-object-localization-challenge>

3.1. Variable Top- k Multi-label Predictions

Conventional multi-class classification models with softmax outputs are limited by their top-1 prediction capability, which is insufficient for datasets where instances could belong to multiple classes. Existing approaches, such as top-5 accuracy and ReaL accuracy, aim to assess the MLPC of models pre-trained on ImageNet but have limitations in their discriminative power when comparing models with similar effectiveness. Both approaches only determine whether the top prediction is in the valid label set for a datapoint; the other possible valid predictions are not taken into account. To address these shortcomings, we propose a variable top- k selection mechanism, where k is derived from the number of valid ground-truth labels for each image. This approach allows us to generate a multi-label prediction set to evaluate the MLPC of models pre-trained on ImageNet by utilizing the metrics explained in Section 3.3.

Given a set of datapoints $\mathbf{X} = \{\mathbf{x}_1, \mathbf{x}_2, \dots, \mathbf{x}_N\}$ and their corresponding softmax outputs $\hat{\mathbf{Y}} = \{\hat{\mathbf{y}}_1, \hat{\mathbf{y}}_2, \dots, \hat{\mathbf{y}}_N\}$, with $\hat{\mathbf{y}}_i \in \mathbb{R}^C$ representing the predicted probability distribution over C classes for the i -th datapoint, we define k_i as the number of ground-truth labels for the i -th datapoint in the test set. For each datapoint \mathbf{x}_i , the top- k_i predictions are obtained by selecting the indices corresponding to the highest k_i values in $\hat{\mathbf{y}}_i$.

3.2. Patch-based Multi-Label Dataset Generation

In Section 2, we discussed prior work that published multi-label annotations for the ImageNetV1 and ImageNetV2 datasets. While these annotations allow evaluating the multi-label capability of models pre-trained on ImageNet, two limitations arise. First, images with higher label counts, such as those with five labels, are too few to ensure reliable assessments of effectiveness. Second, the presence of multiple labels in an image often reflects semantic relationships, which can lead models to learn spurious correlations. Ideally, we seek to assess the ability of models to predict multiple labels even in the absence of semantic relationships between them. Therefore, we propose a methodology to generate a synthesized multi-label evaluation dataset from the object annotations provided by the Image Object Localization Challenge. We refer to the synthesized multi-label dataset as the **Patch-based Multi-Label** (PatchML) dataset.

Our approach was inspired by two established data augmentation techniques: Random Image Cropping and Patching (RICAP) [25] and CutMix [34], both of which involve patch-based image manipulation (Figure 3). While these methods randomly crop image patches, our technique performs targeted cropping of complete objects. The visual illustration of the PatchML dataset creation process is presented in Figure 2.

The PatchML dataset creation process is organized into two main stages: (1) Patch Extraction and Aggregation,

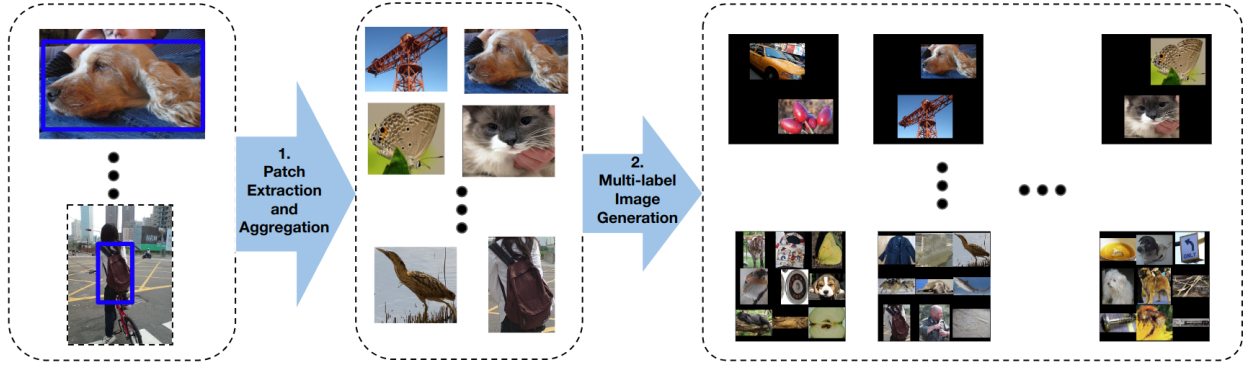


Figure 2. An illustration of the PatchML dataset creation process, organized into two main stages: (1) Patch Extraction and Aggregation, where object regions are cropped and pooled; and (2) Multi-label Image Generation, where a predefined number of patches are randomly sampled without replacement and placed on blank backgrounds to create new multi-label images with corresponding ground-truth label sets.

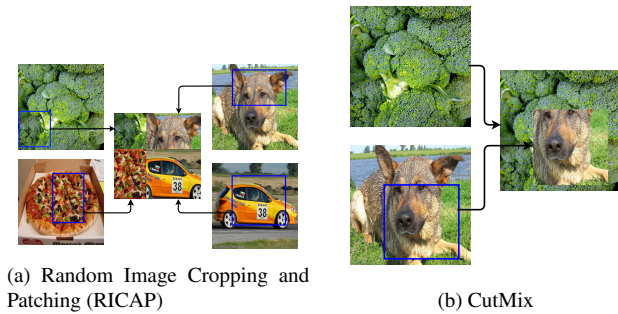


Figure 3. Illustrations of data augmentation techniques that inspired PatchML dataset creation: Random Image Cropping and Patching (RICAP) and CutMix.

and (2) Multi-label Image Generation. In stage 1, given an annotated image dataset with object locations, we crop regions corresponding to each object to create a common pool of patches. In stage 2, for each predefined patch count $k \in \{2, 3, 4, 6, 9\}$, we iteratively create multi-label images by randomly sampling k patches without replacement from the pool. Each patch is resized proportionally to fit within a predefined square box (ranging from 128×128 to 256×256 pixels depending on k), placed randomly within this box, and then positioned on a 512×512 black canvas, ensuring no overlap between objects. The ground-truth labels for each generated image are derived from the union of labels of its constituent patches. The detailed algorithm is provided in Section 6 in the supplementary material.

The PatchML dataset creation process leverages bounding-box annotations to create precise, localized patch combinations of objects, resulting in a high-quality multi-label dataset with novel object combinations not present in the original data. This approach generates a new distribution of multi-label test datapoints that differs

fundamentally from the single-label training data. By introducing these controlled variations, PatchML enables rigorous evaluation of the generalization capabilities of pre-trained DNNs to multi-label scenarios, providing valuable insights into model adaptability and robustness.

To validate the effectiveness of the PatchML dataset for assessing the MLPC of single-label pre-trained DNNs, we perform extensive experiments, which are detailed in Section 4. We argue that the presence of boundary artifacts introduced by combining patches should not necessarily hinder the MLPC assessment, as these artifacts can be considered a form of noise or an artifact that effective DNNs should be able to handle.

3.3. Model Assessment Methodology

After obtaining multi-label predictions from DNNs pre-trained on ImageNet, we employed three key metrics to assess their MLPC: top-1 accuracy, ReaL accuracy, and average subgroup multi-label accuracy (ASMA). These metrics were chosen to provide a comprehensive evaluation while maintaining consistency with conventional classification assessment approaches.

Top-1 Accuracy The top-1 accuracy metric, widely used in multi-class classification, measures the proportion of datapoints for which the highest predicted label of a model matches the single ground-truth label. Formally, for each datapoint \mathbf{x}_i , with predicted label \hat{y}_i and ground-truth label y_i^{gt} , top-1 accuracy is defined as: $\frac{1}{N} \sum_{i=1}^N \mathbb{I}(\hat{y}_i = y_i^{\text{gt}})$, where $\mathbb{I}(\cdot)$ is the indicator function, and N is the total number of datapoints. This formulation aligns with traditional definitions of accuracy used in multi-class settings, such as those discussed by Deng et al. [7] in the context of ImageNet evaluation.

ReaL Accuracy The ReaL accuracy extends top-1 accuracy by accepting matches with any label from an expanded set of plausible ground-truth labels. This metric, introduced by Beyer et al. [3], better handles cases where multiple valid labels exist. Formally, for a datapoint \mathbf{x}_i with predicted label \hat{y}_i and plausible label set $\mathbf{y}_i^{\text{plaus}}$, the ReaL accuracy is computed as: $\frac{1}{N} \sum_{i=1}^N \mathbb{I}(\hat{y}_i \in \mathbf{y}_i^{\text{plaus}})$.

Average Subgroup Multi-Label Accuracy To address the imbalance in the distribution of label counts in multi-label datasets, we introduce ASMA, extending the example-based accuracy metric from multi-label learning [35].

We define subgroups based on the number of labels in each datapoint. For a dataset with C classes, let datapoint $\mathbf{x}_{g,i}$ in subgroup g have ground-truth labels $\mathbf{y}_{g,i}^{\text{gt}} \in \{0, 1\}^C$ and predictions $\hat{\mathbf{y}}_{g,i} \in \{0, 1\}^C$, where $i \in \{1, \dots, N_g\}$ and N_g is the number of datapoints in subgroup g . Each subgroup g contains all datapoints with exactly g labels, where g ranges from 0 to the maximum number of labels in any datapoint.

The label-wise accuracy for a datapoint is $\frac{1}{C} \sum_{c=1}^C \mathbb{I}(y_{g,i,c}^{\text{gt}} = \hat{y}_{g,i,c})$, where $\mathbb{I}(\cdot)$ is the indicator function. The subgroup accuracy A_g averages this across all datapoints in subgroup g : $A_g = \frac{1}{N_g} \sum_{i=1}^{N_g} \frac{1}{C} \sum_{c=1}^C \mathbb{I}(y_{g,i,c}^{\text{gt}} = \hat{y}_{g,i,c})$. The ASMA is then computed as the mean of all subgroup accuracies: $ASMA = \frac{1}{G} \sum_{g=0}^{G-1} A_g$, where G is the number of subgroups defined by the maximum label count observed in the dataset.

4. Experiments and Results

4.1. Experimental Setup

Table 1. The number of images per label count for the ImageNetV1 and ImageNetV2 datasets. For ImageNetV1, we used the ReaL labels [3], which provided refined annotations for 46,837 out of the 50,000 available images in the ImageNetV1 dataset. For ImageNetV2, we used the annotations created by Anzaku et al. [2], totaling 9,858 images from the ImageNetV2 dataset.

Dataset	Label Count					
	1	2	3	4	5	>5
ImageNetV1	39,394	5,408	1,319	411	161	144
ImageNetV2	5,083	2,385	1,306	628	237	232

Test Dataset Description We utilized three datasets to assess the pre-trained DNNs in this study. These datasets were introduced in Section 2 and are the ImageNetV1, ImageNetV2, and PatchML test datasets. The ImageNetV1 is the validation set of the ImageNet-1K dataset that comprises 50,000 images. We used the original single-label

Table 2. The number of images per label count across the PatchML dataset variants.

Dataset	Label Count				
	2	3	4	6	9
PatchML1	26,778	17,870	13,281	8,766	5,736
PatchML2	26,790	17,840	13,306	8,787	5,739
PatchML3	26,777	17,874	13,282	8,760	5,718
PatchML4	26,793	17,852	13,296	8,746	5,721
PatchML5	26,786	17,853	13,296	8,784	5,731

ground-truth labels for this dataset to compute top-1 accuracy and used the ReaL labels [3] to compute the ReaL accuracy. For ImageNetV2, we used the refined labels generated by Anzaku et al. [2], which account for multi-label images. The PatchML data set was created from ImageNetV1 and the available object detection annotations following the methodology described in Section 3.2. The details of the implementation are provided in Section A in the Supplemental Material. The total number of images of the ImageNet-related datasets across different label counts is provided in Table 1. Table 2 presents the information for the generated PatchML datasets using five different seeds.

Description of Assessed Models The evaluated models consist of 315 checkpoints from the popular TIMM repository [30], capturing a wide array of architectures, including convolutional neural networks (CNNs) like ResNet [11], EfficientNet [26], and MobileNet [13], alongside more recent CNN-based and attention-based models such as ConvNeXt V2 [32], Vision Transformers (ViTs) [8], and Swin Transformers [14]. These models represent different configurations where multiple checkpoints may exist for the same architecture due to varying training setups, optimizations, or fine-tuning procedures. The models were primarily trained on or fine-tuned using ImageNet-1K. Some models were pre-trained on larger datasets like ImageNet-22k or JFT-300M [22], which have substantially more training data and diverse categories. This variety in training datasets helps create a broader range of learned representations, contributing to the robustness of model evaluation across different tasks and domains. In particular, this diversity in terms of training data and architectures creates a rich basis for assessing model effectiveness in terms of accuracy across various settings. We first selected the top 100 checkpoints according to the top-1 accuracy on ImageNetV1. The remaining 215 checkpoints were randomly selected to cover a wider range of effectiveness. We provide the names of all the checkpoints and highlight some key characteristics in Section 7 in the supplementary material.

4.2. Results

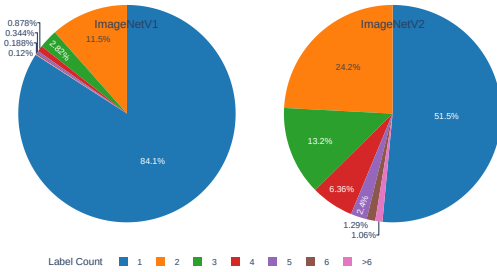


Figure 4. Distribution of images by number of ground-truth labels in ImageNetV1 and ImageNetV2, with images having more than five labels grouped as “> 5”.

Proportion of Multi-label Images The proportion of multi-label images for ImageNetV1 and ImageNetV2 is shown in Figure 4, represented as a pie chart that illustrates the distribution of images by label count. The results clearly show that ImageNetV2 contains a higher proportion of multi-label images, with approximately 48% of its images having more than one label, compared to around 16% for ImageNetV1. Table 1 provides further details on the number of images for each label count across both datasets. While a few of the studies mentioned in Section 2 have explored the multi-label nature of these datasets, none have done so at the scale presented here. In the following sections, we will discuss the results and implications of the differences in the proportion of multi-label images between these datasets.

Accuracy Analysis on ImageNetV1 and ImageNetV2 While the top-1 accuracy is widely used in image recognition, overreliance on this single metric can lead to incomplete conclusions. Figure 5a shows a line graph of the top-1 accuracy across 315 pre-trained DNNs on ImageNetV1 (blue) and ImageNetV2 (orange), with the absolute accuracy difference for each model in red. This plot confirms the observed degradation on ImageNetV2, as discussed in Section 2. However, when accounting for multiple labels using ReaL accuracy and ASMA – calculated for samples with one to five labels to ensure comparability (Figures 5b and 5c) – the gap between the datasets narrows and sometimes disappears. These results suggest that, under the MLPC evaluation, the effectiveness of the model does not exhibit the degradation seen with the accuracy of top-1.

ReaL accuracy and ASMA provide aggregate metrics for a high-level overview of effectiveness. To gain a more detailed understanding of MLPC w.r.t. label count, we present

boxplots in Figure 6 for ReaL and subgroup accuracy. Each box summarizes the model accuracies for a specific label count, with blue and orange boxes representing ImageNetV1 and ImageNetV2, respectively. Individual subgroup accuracies are plotted as dots across the different label counts.

Several key observations emerge: First, the accuracy distributions for both datasets are similar, with a higher median accuracy for ImageNetV2 under ReaL accuracy for label counts greater than two. Second, the range of MLPC between models varies widely, indicating that the MLPC assessment captures substantial differences in effectiveness among the models. However, Table 1 shows that the number of images with certain label counts is low, potentially introducing uncertainty in the results. To address this, we further explore MLPC using the PatchML dataset in the next section.

The MLPC of Pre-Trained Models on the PatchML Test Dataset We present a box plot of subgroup accuracy versus label count for the five PatchML datasets in Figure 7, each generated using a different seed. In the plot, each dot represents the subgroup accuracy of a model for one of the PatchML datasets, resulting in five dots per label count for each model. The plot demonstrates that models pre-trained on single-label tasks can reasonably predict multiple labels, highlighting their capacity for multi-label classification. Furthermore, this figure confirms the results shown in Figure 6, which illustrate the wide range of MLPC between models. Compared to Figure 6, Figure 7 shows lower median accuracies, potentially due to differences in label distribution and the disruption of semantic relationships between labels in the PatchML datasets.

To further illustrate that the top-1 accuracy overlooks certain desirable properties, such as the ability of models to predict multiple labels in an image, we present two key comparisons. First, Figure 7 overlays line plots on the boxplots, showing the top-5 models ranked by ImageNetV1 top-1 accuracy (blue) and PatchML ASMA (orange). This visualization highlights how models that perform well under top-1 accuracy may not excel in predicting multiple labels, as reflected in their lower subgroup accuracy scores. Second, Table 3 lists the top-10 models sorted by PatchML ASMA, providing their top-1 accuracy, ASMA scores, top-1 ranks, and the change in rank between top-1 and ASMA. The results presented in Table 3 demonstrate that models with higher ASMA scores show substantial improvements in rank compared to their top-1 accuracy rankings, emphasizing the importance of considering multi-label metrics for a more nuanced assessment of model effectiveness. The ASMA presented in the table is the average ASMA for each model across the five PatchML datasets assessed.

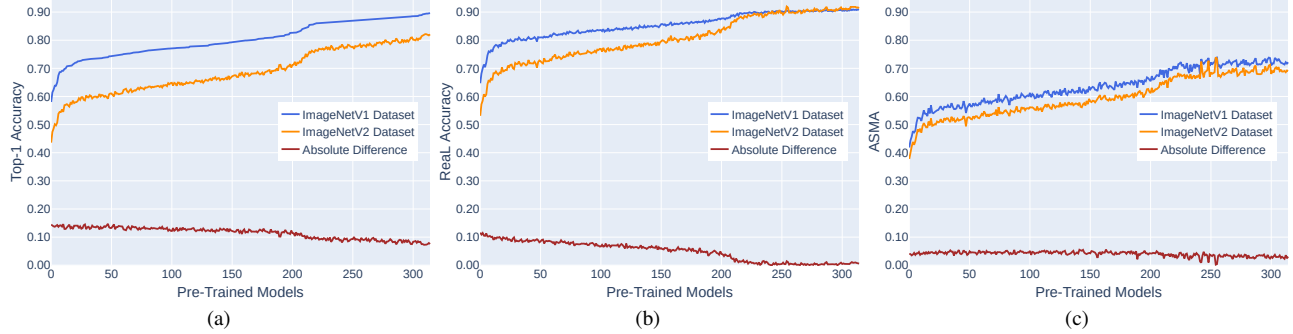


Figure 5. Accuracies obtained by assessing 315 pre-trained DNNs on *ImageNetV1* and *ImageNetV2*: (a) Top-1 Accuracy, (b) Real Accuracy, and (c) ASMA, all plotted against label count. The absolute difference represents the accuracy difference between the two datasets. Models in all plots are sorted by Top-1 accuracy on *ImageNetV1*.

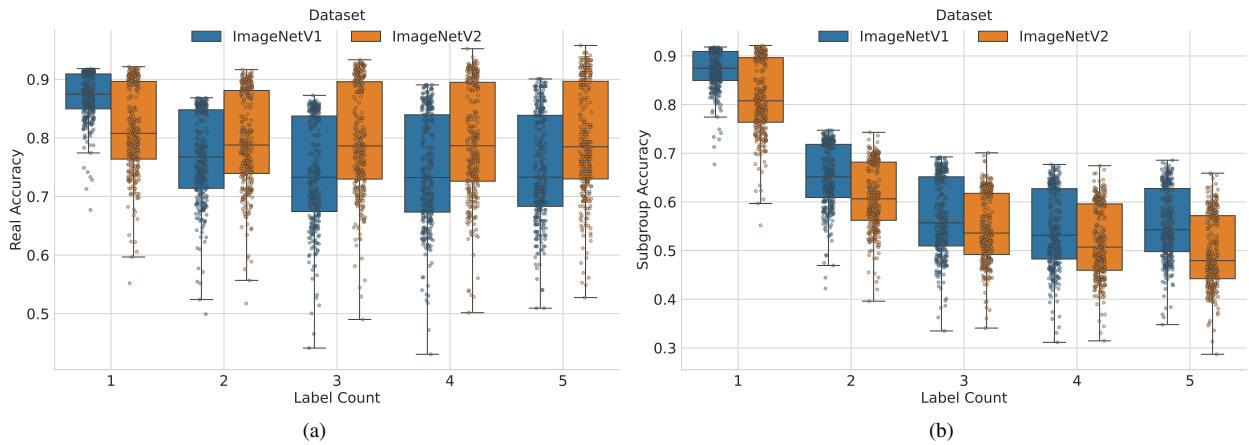


Figure 6. Effectiveness distribution of 315 DNNs pre-trained on *ImageNet*, with effectiveness obtained on *ImageNetV1* and *ImageNetV2* (for datapoints with 1-5 labels): (a) Real Accuracy and (b) Subgroup Accuracy versus Label Count. Each dot represents the accuracy of a model for images with the corresponding label count.

Table 3. Effectiveness and rank changes of the top-10 checkpoints based on ASMA on PatchML. Δ Rank indicates their ranking shift between top-1 accuracy on *ImageNetV1* and ASMA on PatchML.

Model Checkpoint	ImageNetV1		PatchML	Δ Rank
	Top-1	Rank	ASMA	
eva_large_patch14_336.in22k_ft.in1k	88.50	14	74.50	+13
convnextv2_huge.fcmae.ft.in22k.in1k_512	88.84	8	71.45	+6
volo_d5_448.in1k	87.05	56	70.30	+53
volo_d5_512.in1k	87.04	57	70.17	+53
volo_d4_448.in1k	86.86	63	69.18	+58
volo_d3_448.in1k	86.60	69	69.16	+63
convnextv2_huge.fcmae.ft.in22k.in1k_384	88.60	10	67.92	+3
eva_large_patch14_196.in22k_ft.in1k	87.77	36	67.20	+28
beitv2_large_patch16_224.in1k_ft.in1k	87.23	51	67.16	+42
cait_m48_448.fb_dist.in1k	86.32	81	67.11	+71

5. Conclusions

ImageNet remains a fundamental benchmark for computer vision research, particularly for evaluating model capabilities beyond single-label classification. Ensuring that ima-

genet benchmarking accurately reflects the nuanced capabilities of DNNs is crucial to steer research in the right direction. In this work, we critically examine the prevailing single-label assumption in *ImageNet* benchmarking and its role in the reported unexpected and largely unexplained degradation in effectiveness observed in *ImageNetV2*. By embracing a multi-label perspective, we found that a critical understudied factor in the reported accuracy degradation is the difference in the proportion of multi-label datapoints between *ImageNetV1* and *ImageNetV2*, a finding that has been obscured by the typical use of a single-label evaluation approach. Our experimental results did not find support for the reported substantial degradation in effectiveness observed in *ImageNetV2*. In contrast, we found that *ImageNet* pre-trained DNNs, on average, perform equally well or even better on *ImageNetV2*. Our analysis reveals that single-label evaluation fails to capture the inherent complexity of the *ImageNet* dataset. By solely focusing on single-label classification, there is a risk of drawing incom-

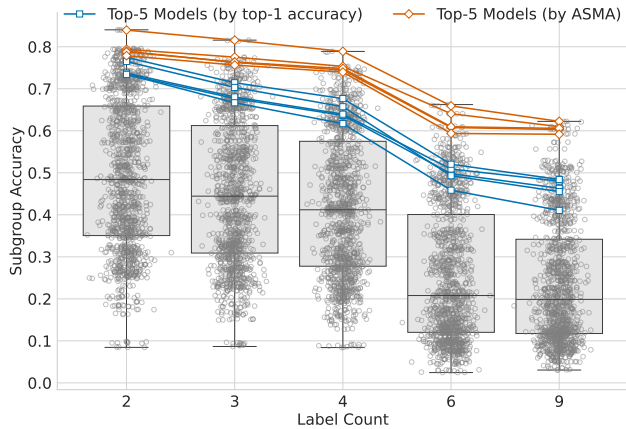


Figure 7. Subgroup accuracy box plot for 315 pre-trained DNNs evaluated on PatchML. Overlaid are line plots for the top-5 models based on ImageNetV1 top-1 accuracy (blue) and PatchML ASMA (orange).

plete or even misleading conclusions about the effectiveness of DNNs. Such oversights may obscure a comprehensive understanding of DNN capabilities and could inadvertently redirect research efforts away from crucial considerations surrounding the reliability and generalizability of DNNs. Therefore, we advocate for the adoption of a multi-label evaluation approach in future ImageNet benchmarking practices, believing that this approach will foster advancements in computer vision that are more aligned with the complexities of the real world.

References

- [1] Esla Timothy Anzaku, Haohan Wang, Arnout Van Messem, and Wesley De Neve. A Principled Evaluation Protocol for Comparative Investigation of the Effectiveness of DNN Classification Models on Similar-but-non-identical Datasets, 2022. 3
- [2] Esla Timothy Anzaku, Hyesoo Hong, Jin-Woo Park, Wonjun Yang, Kangmin Kim, JongBum Won, Deshika Vinoshani Kumari Herath, Arnout Van Messem, and Wesley De Neve. Leveraging Human-Machine Interactions for Computer Vision Dataset Quality Enhancement. In *Intelligent Human Computer Interaction*, pages 295–309, 2024. 3, 6
- [3] Lucas Beyer, Olivier J. Hénaff, Alexander Kolesnikov, Xiaohua Zhai, and Aäron van den Oord. Are we done with ImageNet?, 2020. 1, 3, 6
- [4] Ting Chen, Simon Kornblith, Mohammad Norouzi, and Geoffrey Hinton. A Simple Framework for Contrastive Learning of Visual Representations. In *International Conference on Machine Learning*, pages 1597–1607, 2020. ISSN: 2640-3498. 1
- [5] Zhe Chen, Jiannan Wu, Wenhai Wang, Weijie Su, Guo Chen, Sen Xing, Muyan Zhong, Qinglong Zhang, Xizhou Zhu, Lewei Lu, Bin Li, Ping Luo, Tong Lu, Yu Qiao, and Jifeng Dai. Intern VL: Scaling up Vision Foundation Models and Aligning for Generic Visual-Linguistic Tasks. In *2024 IEEE/CVF Conference on Computer Vision and Pattern Recognition (CVPR)*, pages 24185–24198, Seattle, WA, USA, 2024. IEEE. 1
- [6] Elijah Cole, Oisín Mac Aodha, Titouan Lorieul, Pietro Perona, Dan Morris, and Nebojsa Jojic. Multi-Label Learning from Single Positive Labels. In *IEEE/CVF Conference on Computer Vision and Pattern Recognition*, pages 933–942, 2021. 4
- [7] Lei Deng, Youzhi Liu, Yechuan Shi, Wenhao Zhang, Chun Yang, and Hui Liu. Deep neural networks for inferring binding sites of RNA-binding proteins by using distributed representations of RNA primary sequence and secondary structure. *BMC Genomics*, 21(13):866, 2020. 1, 5
- [8] Alexey Dosovitskiy, Lucas Beyer, Alexander Kolesnikov, Dirk Weissenborn, Xiaohua Zhai, Thomas Unterthiner, Mostafa Dehghani, Matthias Minderer, Georg Heigold, Sylvain Gelly, Jakob Uszkoreit, and Neil Houlsby. An Image is Worth 16x16 Words: Transformers for Image Recognition at Scale. In *Ninth International Conference on Learning Representations*, 2021. 1, 6
- [9] Logan Engstrom, Andrew Ilyas, Shibani Santurkar, Dimitris Tsipras, Jacob Steinhardt, and Aleksander Madry. Identifying Statistical Bias in Dataset Replication. In *Proceedings of the 37th International Conference on Machine Learning*, pages 2922–2932, 2020. 3
- [10] Jean-Bastien Grill, Florian Strub, Florent Altché, Corentin Tallec, Pierre Richemond, Elena Buchatskaya, Carl Doersch, Bernardo Avila Pires, Zhaohan Guo, Mohammad Gheshlaghi Azar, Bilal Piot, Koray Kavukcuoglu, Remi Munos, and Michal Valko. Bootstrap Your Own Latent - A New Approach to Self-Supervised Learning. In *Advances in Neural Information Processing Systems*, pages 21271–21284, 2020. 1
- [11] Kaiming He, Xiangyu Zhang, Shaoqing Ren, and Jian Sun. Deep Residual Learning for Image Recognition. In *IEEE Conference on Computer Vision and Pattern Recognition*, pages 770–778, 2016. 1, 6
- [12] Kaiming He, Xinlei Chen, Saining Xie, Yanghao Li, Piotr Dollár, and Ross Girshick. Masked Autoencoders Are Scalable Vision Learners. In *IEEE/CVF Conference on Computer Vision and Pattern Recognition (CVPR)*, pages 15979–15988, 2022. 1
- [13] Andrew G. Howard, Menglong Zhu, Bo Chen, Dmitry Kalenichenko, Weijun Wang, Tobias Weyand, Marco Andreetto, and Hartwig Adam. MobileNets: Efficient Convolutional Neural Networks for Mobile Vision Applications, 2017. 6
- [14] Ze Liu, Yutong Lin, Yue Cao, Han Hu, Yixuan Wei, Zheng Zhang, Stephen Lin, and Baining Guo. Swin Transformer: Hierarchical Vision Transformer using Shifted Windows. In *IEEE/CVF International Conference on Computer Vision*, pages 9992–10002, 2021. 6
- [15] Zhuang Liu, Hanzi Mao, Chao-Yuan Wu, Christoph Feichtenhofer, Trevor Darrell, and Saining Xie. A ConvNet for the 2020s. In *The IEEE / CVF Computer Vision and Pattern Recognition Conference*, pages 11966–11976, 2022. 1

- [16] Maxime Oquab, Timothée Darcet, Théo Moutakanni, Huy V Vo, Marc Szafranec, Vasil Khalidov, Pierre Fernandez, Daniel Haziza, Francisco Massa, Alaaeldin El-Nouby, Mahmoud Assran, Nicolas Ballas, Wojciech Galuba, Russell Howes, Po-Yao Huang, Shang-Wen Li, Ishan Misra, Michael Rabbat, Vasu Sharma, Gabriel Synnaeve, Hu Xu, Hervé Jegou, Julien Mairal, Patrick Labatut, Armand Joulin, and Piotr Bojanowski. DINOv2: Learning Robust Visual Features without Supervision. *Transactions on Machine Learning Research*, 2024. 1
- [17] Alec Radford, Jong Wook Kim, Chris Hallacy, Aditya Ramesh, Gabriel Goh, Sandhini Agarwal, Girish Sastry, Amanda Askell, Pamela Mishkin, Jack Clark, Gretchen Krueger, and Ilya Sutskever. Learning Transferable Visual Models From Natural Language Supervision. In *Proceedings of the 38th International Conference on Machine Learning*, pages 8748–8763, 2021. 1
- [18] Benjamin Recht, Rebecca Roelofs, Ludwig Schmidt, and Vaishaal Shankar. Do ImageNet Classifiers Generalize to ImageNet? In *Proceedings of the 36th International Conference on Machine Learning*, pages 5389–5400, 2019. 2, 3
- [19] Olga Russakovsky, Jia Deng, Hao Su, Jonathan Krause, Sanjeev Satheesh, Sean Ma, Zhiheng Huang, Andrej Karpathy, Aditya Khosla, Michael Bernstein, Alexander C. Berg, and Li Fei-Fei. ImageNet Large Scale Visual Recognition Challenge. *International Journal of Computer Vision*, 115(3): 211–252, 2015. 1
- [20] Vaishaal Shankar, Rebecca Roelofs, Horía Mania, Alex Fang, Benjamin Recht, and Ludwig Schmidt. Evaluating Machine Accuracy on ImageNet. In *International Conference on Machine Learning*, pages 8634–8644, 2020. ISSN: 2640-3498. 1, 3
- [21] Pierre Stock and Moustapha Cisse. ConvNets and ImageNet Beyond Accuracy: Understanding Mistakes and Uncovering Biases. In *The European Conference on Computer Vision*, pages 504–519, 2018. 3
- [22] Chen Sun, Abhinav Shrivastava, Saurabh Singh, and Abhinav Gupta. Revisiting Unreasonable Effectiveness of Data in Deep Learning Era. In *IEEE International Conference on Computer Vision*, pages 843–852, 2017. 6
- [23] Quan Sun, Yuxin Fang, Ledell Wu, Xinlong Wang, and Yue Cao. EVA-CLIP: Improved Training Techniques for CLIP at Scale, 2023. 1
- [24] Mohammad Reza Taesiri, Giang Nguyen, Sarra Habchi, Cor-Paul Bezemer, and Anh Nguyen. ImageNet-Hard: The Hardest Images Remaining from a Study of the Power of Zoom and Spatial Biases in Image Classification. In *Conference on Neural Information Processing Systems*, 2023. 3
- [25] Ryo Takahashi, Takashi Matsubara, and Kuniaki Uehara. RICAP: Random Image Cropping and Patching Data Augmentation for Deep CNNs. In *Proceedings of The 10th Asian Conference on Machine Learning*, pages 786–798, 2018. 4
- [26] Mingxing Tan and Quoc V. Le. EfficientNet: Rethinking Model Scaling for Convolutional Neural Networks. In *Proceedings of the 36th International Conference on Machine Learning*, pages 6105–6114, 2019. 6
- [27] Dimitris Tsipras, Shibani Santurkar, Logan Engstrom, Andrew Ilyas, and Aleksander Madry. From ImageNet to Image Classification: Contextualizing Progress on Benchmarks. In *International Conference on Machine Learning*, pages 9625–9635, 2020. 2, 3
- [28] Vijay Vasudevan, Benjamin Caine, Raphael Gontijo-Lopes, Sara Fridovich-Keil, and Rebecca Roelofs. When does dough become a bagel? Analyzing the remaining mistakes on ImageNet. In *Conference on Neural Information Processing Systems*, 2022. 3
- [29] Thomas Verelst, Paul K. Rubenstein, Marcin Eichner, Tinne Tuytelaars, and Maxim Berman. Spatial Consistency Loss for Training Multi-Label Classifiers from Single-Label Annotations. In *IEEE/CVF Winter Conference on Applications of Computer Vision*, pages 3868–3878, 2023. 4
- [30] Ross Wightman. PyTorch Image Models, 2019. Publication Title: GitHub repository. 6, 11
- [31] Ross Wightman, Ross. Pytorch Image Models, 2019. 2
- [32] Sanghyun Woo, Shoubhik Debnath, Ronghang Hu, Xinlei Chen, Zhuang Liu, In So Kweon, and Saining Xie. ConvNeXt V2: Co-designing and Scaling ConvNets with Masked Autoencoders. In *IEEE/CVF Conference on Computer Vision and Pattern Recognition*, pages 16133–16142, 2023. 6
- [33] Li Yuan, Qibin Hou, Zihang Jiang, Jiashi Feng, and Shuicheng Yan. VOLO: Vision Outlooker for Visual Recognition. *IEEE Transactions on Pattern Analysis and Machine Intelligence*, 45(5):6575–6586, 2023. Conference Name: IEEE Transactions on Pattern Analysis and Machine Intelligence. 2
- [34] Sangdoon Yun, Dongyoon Han, Seong Joon Oh, Sanghyuk Chun, Junsuk Choe, and Youngjoon Yoo. CutMix: Regularization Strategy to Train Strong Classifiers with Localizable Features. In *International Conference on Computer Vision (ICCV)*, 2019. 4
- [35] Min-Ling Zhang and Zhi-Hua Zhou. A Review on Multi-Label Learning Algorithms. *IEEE Transactions on Knowledge and Data Engineering*, 26(8):1819–1837, 2014. 6

A. PatchML Dataset Generation Process

The PatchML dataset generation involves two key stages: *Patch Extraction and Aggregation* and *Multi-label Image Generation*. In the first stage, object regions are cropped from annotated source images to form a labeled pool of patches. The second stage, described in Algorithm 1, constructs multi-label composite images from these patches.

Algorithm 1 takes four key inputs: the pool of extracted patches S , a list of patch counts K , corresponding patch sizes P , and the final image size F . We utilized $F = 512$, $K = [2, 3, 4, 6, 9]$, and $P = [256, 256, 256, 170, 128]$ to generate composite multi-label images of 512×512 resolution.

For each configuration (k, p) , where $k \in K$ and $p \in P$, the algorithm ensures that patches fit within the final $F \times F$ image by validating two conditions: (1) the total patch area $k p^2$ must not exceed the final image area F^2 , and (2) the number of patches k must not exceed the grid capacity c^2 , where $c = \lfloor F/p \rfloor$ represents the number of columns. Since the images are square, the number of rows is equal to c .

The multi-label composite image generation process iterates while sufficient patches remain in the pool, i.e., while $|S| \geq k$.

For each iteration:

1. A black canvas I_{new} of size $F \times F$ is initialized
2. k patches are randomly sampled without replacement from S
3. Each sampled patch is processed sequentially through the PLACEPATCHINTOGRID function, which:
 - Calculates the grid position based on the patch index
 - Resizes the patch to the specified size p
 - Randomly offsets the patch within its grid cell to introduce positioning variety
 - Places the patch if boundary conditions are satisfied
 - Tracks used grid cells to prevent overlaps

The final label set for each composite image is the union of labels from successfully placed patches. The process maintains dataset diversity by removing used patches from the pool after each composite image generation.

This two-stage approach combines precise patch extraction with systematic placement to ensure dataset quality. The grid-based strategy enforces structure while allowing controlled randomization, resulting in diverse multi-label images without patch overlaps.

B. Summary of Assessed Pre-Trained DNNs

We evaluated 315 pre-trained checkpoints from the Timm Repository [30] to ensure a comprehensive assessment. The selection included the top-100 checkpoints ranked by top-1 accuracy, along with an additional 215 randomly selected checkpoints to capture a diverse range of top-1 accuracy effectiveness levels.

Our assessment used consistent image transformations across all checkpoints, maintaining their default input image sizes. To eliminate potential center bias in multi-label prediction evaluation, we employed only image resizing and omitted the standard center-cropping step.

The checkpoint assessment results for all checkpoints are detailed in Tables 4 through 10, showing model effectiveness using three metrics (top-1 accuracy, ReaL accuracy, and ASMA) across the ImageNetV1, ImageNetV2, and PatchML datasets. The tables also present ΔRank , which measures the shift in model rankings between top-1 accuracy on ImageNetV1 and ASMA on PatchML. Notably, many models demonstrated improved rankings when evaluated using ASMA on PatchML.

C. Examples of PatchML Predictions

Section 4 demonstrated that single-label pre-trained ImageNet models exhibit MLPC, as shown by the subgroup accuracy analysis in Figure 7. To further illustrate this capability, even for images containing nine objects, Figure 8 presents example predictions from the top-performing model identified in Table 3. For each example, the input image appears on the left with its corresponding predictions on the right. Green bars indicate correct predictions (those matching the ground-truth label set), while red bars denote incorrect predictions.

Algorithm 1 Multi-label Dataset Generation System

1: **procedure** GENERATEPATCHMLDATASET(S, K, P, F)

Require:

- 2: S : Set of patches with their corresponding labels
- 3: K : List of unique patch counts per image (e.g., [2, 3, 4, 6, 9])
- 4: P : Corresponding list of patch sizes (e.g., [256, 256, 256, 170, 128])
- 5: F : Final image size (e.g., 512×512)

Ensure: D : Dictionary mapping composite image names to their list of labels

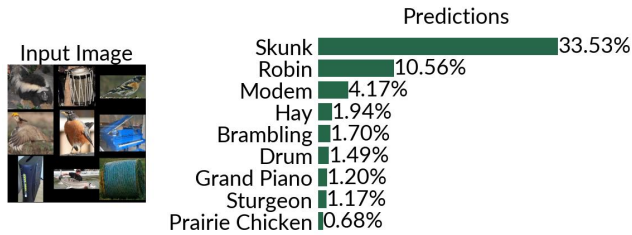
```
6:    $D \leftarrow \emptyset$ 
7:   for each  $(k, p)$  in zip( $K, P$ ) do
8:      $c \leftarrow \lfloor F/p \rfloor$ 
9:      $n \leftarrow c^2$ 
10:    if  $k \cdot p^2 > F^2$  or  $k > n$  then
11:      raise error: Configuration invalid
12:    end if
13:    while  $|S| \geq k$  do
14:       $I_{\text{new}} \leftarrow \text{zeros}(F \times F)$ 
15:       $S_k \leftarrow \text{random\_sample}(S, k)$ 
16:       $U \leftarrow \emptyset$ 
17:       $L \leftarrow \emptyset$ 
18:      for  $i \leftarrow 0$  to  $k - 1$  do
19:         $s \leftarrow S_k[i]$ 
20:        success,  $I_{\text{new}}, U \leftarrow \text{PLACEPATCHINGRID}(I_{\text{new}}, s, i, p, c, F, U)$ 
21:        if success then
22:           $L \leftarrow L \cup \{\text{label}(s)\}$ 
23:        end if
24:      end for
25:       $D[\text{name}(I_{\text{new}})] \leftarrow \text{list}(L)$ 
26:       $S \leftarrow S \setminus S_k$ 
27:    end while
28:  end for
29:  return  $D$ 
30: end procedure
```

▷ Initialize an empty data set
▷ Process each patch configuration
▷ Calculate the grid columns
▷ Total available grid cells
▷ Validate the configuration
▷ Process while enough patches remain
▷ Initialize a black canvas
▷ Sample k patches
▷ Track occupied grid cells
▷ Initialize a label collection
▷ Place each patch
▷ Get the current patch
▷ Add the label if placement successful
▷ Store the composite image
▷ Remove used patches
▷ Return the generated dataset

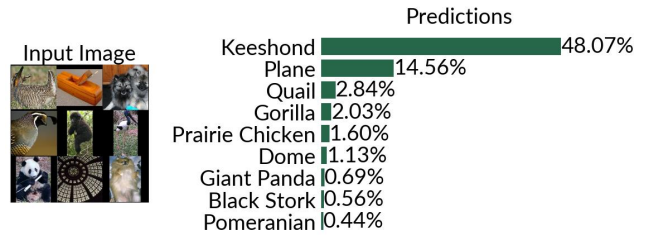
31: **function** PLACEPATCHINTOGRID(I, s, i, p, c, F, U)

```
32:    $\text{row} \leftarrow \lfloor i/c \rfloor$ 
33:    $\text{col} \leftarrow i \bmod c$ 
34:   if  $(\text{row}, \text{col}) \in U$  then
35:     return false,  $I, U$ 
36:   end if
37:    $s' \leftarrow \text{resize}(s, p)$ 
38:    $w, h \leftarrow \text{dimensions}(s')$ 
39:    $x_{\text{max}} \leftarrow p - w$ 
40:    $y_{\text{max}} \leftarrow p - h$ 
41:    $x_{\text{off}} \sim \mathcal{U}(0, x_{\text{max}})$ 
42:    $y_{\text{off}} \sim \mathcal{U}(0, y_{\text{max}})$ 
43:    $x \leftarrow \text{col} \cdot p + x_{\text{off}}$ 
44:    $y \leftarrow \text{row} \cdot p + y_{\text{off}}$ 
45:   if  $x + w \leq F$  and  $y + h \leq F$  then
46:      $I[y : y + h, x : x + w] \leftarrow s'$ 
47:      $U \leftarrow U \cup \{(\text{row}, \text{col})\}$ 
48:     return true,  $I, U$ 
49:   end if
50:   return false,  $I, U$ 
51: end function
```

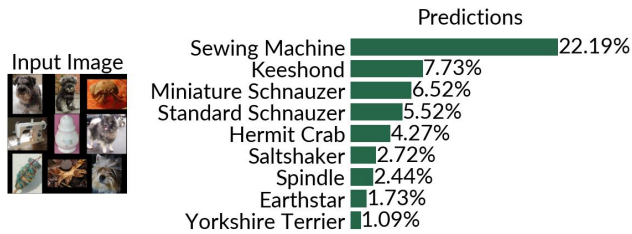
▷ Calculate the grid position
▷ Check if a cell is occupied
▷ Resize the patch
▷ Get the dimensions
▷ Calculate the maximum offsets
▷ Sample random offsets
▷ Calculate the final position
▷ Check the boundary conditions
▷ Place patch
▷ Mark the cell as used
▷ Return a failure if placement is invalid



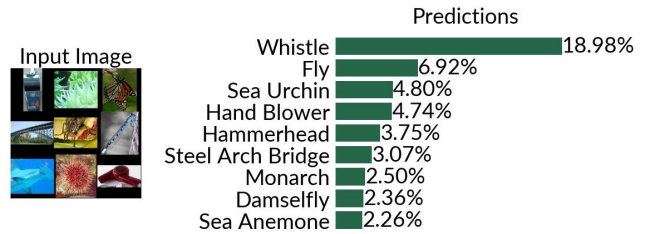
(a) All top-9 predictions exactly match the ground labels.



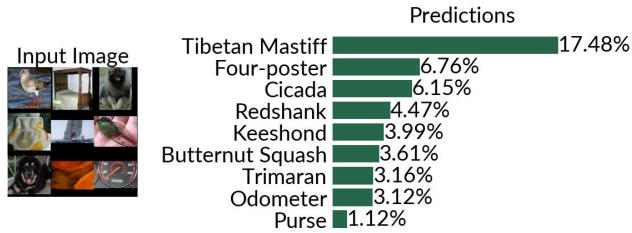
(b) All top-9 predictions exactly match the ground labels.



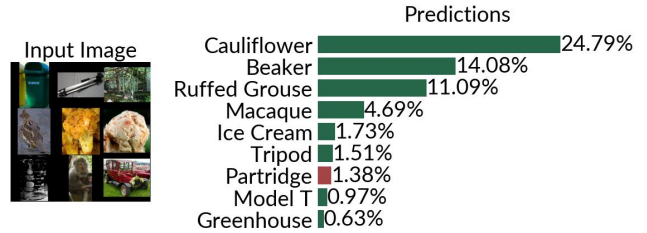
(c) All top-9 predictions exactly match the ground labels.



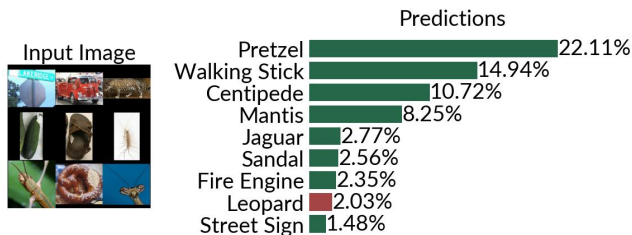
(d) All top-9 predictions exactly match the ground labels.



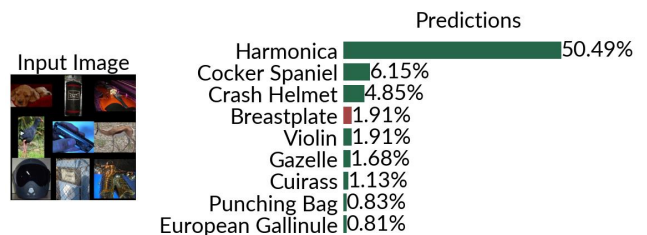
(e) All top-9 predictions exactly match the ground labels.



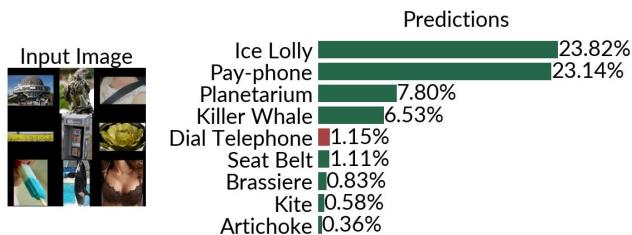
(f) The ground truth label not in the top-9 is *Ash Can*.



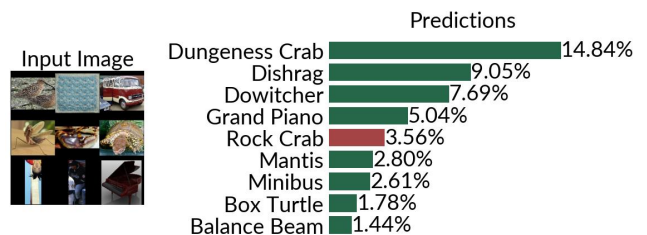
(g) The ground truth label not in the top-9 is *Leopard*.



(h) The ground truth label not in the top-9 is *Gas Pump*.



(i) The ground truth label not in the top-9 is *Rapeseed*.



(j) The ground truth label not in the top-9 is *Ballplayer*.

Figure 8. Examples of PatchML predictions for sample images with nine ground truth labels. Red bars indicate predicted labels that are not part of the ground truth set.

Table 4. Comparing model effectiveness using top-1 accuracy, ReaL accuracy, and ASMA metrics across ImageNetV1 (V1), ImageNetV2 (V2), and PatchML datasets. Models are ordered by ASMA effectiveness on PatchML, with Δ Rank showing their shift from top-1 V1 ranking.

Checkpoint Name	Top-1 Accuracy		ReaL Accuracy		ASMA			Δ Rank
	V1	V2	V1	V2	V1	V2	PatchML	
eva_large_patch14_336.in22k_ft.in1k	88.5	80.99	90.76	91.74	72.22	70.35	74.5	+13
convnextv2_huge.fcmae_ft.in22k.in1k.512	88.84	80.52	90.56	91.05	68.52	68.98	71.45	+6
volo_d5_448.sail.in1k	87.05	78.07	90.46	91.65	71.63	72.39	70.3	+53
volo_d5_512.sail.in1k	87.04	77.87	90.53	92.03	72.34	73.4	70.17	+53
volo_d4_448.sail.in1k	86.86	77.77	90.4	90.8	71.71	70.71	69.18	+58
volo_d3_448.sail.in1k	86.6	77.68	90.32	90.42	71.44	70.06	68.16	+63
convnextv2_huge.fcmae_ft.in22k.in1k.384	88.6	80.06	90.42	90.9	67.71	68.86	67.92	+3
eva_large_patch14_196.in22k_ft.in1k	87.77	80.14	90.58	91.25	71.87	68.13	67.2	+28
beitv2_large_patch16_224.in1k_ft.in1k	87.23	78.1	90.08	89.78	71.64	67.09	67.16	+42
cait_m48_448.fb_dist.in1k	86.32	76.9	90.08	89.51	68.73	63.68	67.11	+71
swinv2_large_window12to24_192to384.ms.in22k_ft.in1k	87.41	77.67	90.18	89.79	68.92	66.07	66.07	+34
deit3_large_patch16_384.fb.in22k_ft.in1k	87.25	77.98	90.05	89.86	72.21	67.6	65.99	+37
maxvit_rmlp_base_rw_384.sw.in12k_ft.in1k	87.83	79.4	90.59	91.1	71.39	65.08	65.5	+22
regnety_1280.swag_ft.in1k	88.3	80.18	90.61	91.15	72.8	68.45	65.42	+4
convnextv2_huge.fcmae_ft.in1k	86.07	76.8	89.92	88.91	71.46	65.82	64.85	+72
maxxvitv2_rmlp_base_rw_384.sw.in12k_ft.in1k	87.47	78.45	90.43	90.64	70.93	69.09	64.78	+28
deit_base_distilled_patch16_384.fb.in1k	85.44	75.53	89.61	88.19	67.62	63.16	64.59	+77
eva_large_patch14_336.in22k_ft.in22k.in1k	88.83	80.62	90.65	91.19	70.56	67.23	64.05	-9
swinv2_base_window12to24_192to384.ms.in22k_ft.in1k	86.82	77.35	90.3	89.49	69.58	67.07	63.88	+48
convformer_b36.sail.in22k_ft.in1k.384	87.57	79.01	90.49	90.94	70.76	68.63	63.81	+21
deit3_base_patch16_384.fb.in22k_ft.in1k	86.15	76.72	89.73	88.59	71.36	65.33	63.79	+65
eva_giant_patch14_560.m30m_ft.in22k.in1k	89.62	81.71	90.92	91.75	71.16	66.21	63.42	-20
swin_large_patch4_window12_384.ms.in22k_ft.in1k	86.97	76.92	90.03	89.08	68.17	65.36	62.67	+38
convnext_xlarge.fb.in22k_ft.in1k.384	87.48	78.18	90.46	90.04	70.95	67.58	62.14	+19
deit3_large_patch16_224.fb.in22k_ft.in1k	86.22	77.04	89.63	88.84	71.71	67.66	61.86	+60
caformer_b36.sail.in22k_ft.in1k.384	88.08	79.95	90.75	91.93	72.01	69.23	61.81	+1
convnext_xxlarge.clip_laion2b_soup_ft.in1k	88.56	80.1	90.56	91.25	69.71	66.69	61.59	-15
eva_giant_patch14_336.m30m_ft.in22k.in1k	89.2	81.69	90.71	91.92	70.63	65.9	61.49	-22
convformer_m36.sail.in22k_ft.in1k.384	87.01	77.75	90.34	90.0	71.25	67.46	61.36	+30
swinv2_large_window12to16_192to256.ms.in22k_ft.in1k	86.39	76.51	89.71	88.71	66.83	64.33	61.31	+49
seresnextaa101d_32x8d.sw.in12k_ft.in1k.288	86.63	77.1	90.14	89.46	69.46	66.12	61.19	+39
eva02_large_patch14_448.mim.in22k_ft.in22k.in1k	89.46	81.94	90.73	91.58	68.31	68.49	60.96	-29
eva02_large_patch14_448.mim_m38m_ft.in1k	89.46	82.12	90.84	91.92	68.53	67.14	60.25	-30
eva02_large_patch14_448.mim_m38m_ft.in22k.in1k	89.62	82.07	90.87	91.52	70.41	67.23	60.16	-33
deit3_huge_patch14_224.fb.in22k_ft.in1k	86.35	77.29	89.78	89.44	69.92	65.58	60.11	+45
convformer_b36.sail.in22k_ft.in1k	86.95	77.67	90.28	89.88	70.46	67.73	59.61	+26
maxvit_base.tf_512.in1k	86.65	77.68	89.97	89.91	70.59	67.87	59.49	+32
convnext_large.fb.in22k_ft.in1k.384	87.24	77.66	90.22	89.54	69.13	64.85	59.36	+13
convnext_base.fb.in22k_ft.in1k.384	86.55	76.92	90.13	89.15	70.21	64.68	59.15	+35
beit_large_patch16_512.in22k_ft.in22k.in1k	88.57	80.58	90.79	91.36	70.57	67.65	59.1	-29
convnextv2_large.fcmae_ft.in22k.in1k.384	87.89	78.6	90.33	90.34	69.23	66.25	59.09	-8
convnextv2_base.fcmae_ft.in22k.in1k.384	87.38	77.84	90.28	89.61	70.58	67.47	59.06	+4
caformer_m36.sail.in22k_ft.in1k.384	87.52	79.08	90.52	90.62	70.21	66.81	58.93	-1
tf_efficientnet_l2.ns.jft.in1k	88.43	80.87	90.69	91.35	72.48	69.07	58.64	-29
maxvit_xlarge.tf_512.in21k_ft.in1k	88.57	79.95	90.47	91.04	70.98	66.76	58.52	-34

Table 5. Comparing model effectiveness using top-1 accuracy, ReaL accuracy, and ASMA metrics across ImageNetV1 (V1), ImageNetV2 (V2), and PatchML datasets. Models are ordered by ASMA effectiveness on PatchML, with Δ Rank showing their shift from top-1 V1 ranking.

Checkpoint Name	Top-1 Accuracy		ReaL Accuracy		ASMA			Δ Rank
	V1	V2	V1	V2	V1	V2	PatchML	
coatnet_rmlp_2_rw_384.sw_in12k_ft_in1k	87.29	78.81	90.33	90.6	69.77	66.62	58.42	+2
maxvit_rmlp_base_rw_224.sw_in12k_ft_in1k	86.74	77.5	89.96	89.61	71.82	63.48	58.34	+21
convnext_large_mlp.clip_laion2b_augreg_ft_in1k_384	87.86	79.13	90.63	90.76	69.21	66.85	58.2	-14
maxvit_large_tf_512.in1k	86.57	77.58	89.81	89.68	70.3	67.57	57.93	+23
eva02_base_patch14_448.mim_in22k_ft_in22k_in1k	88.28	79.28	90.64	90.4	70.68	66.53	57.76	-31
eva02_large_patch14_448.mim_in22k_ft_in1k	89.38	82.16	90.77	91.78	69.22	67.24	57.73	-47
regnety_320.swag_ft_in1k	86.86	78.21	90.2	89.82	72.25	66.0	57.66	+13
deit_base_patch16_384.fb_in1k	82.94	71.82	87.76	84.52	66.57	61.19	57.61	+51
convnext_xlarge.fb_in22k_ft_in1k	86.03	76.41	89.56	88.45	66.69	66.24	57.45	+34
eva_giant_patch14_336.clip_ft_in1k	89.32	82.05	90.93	91.84	71.82	66.61	57.43	-50
eva_large_patch14_196.in22k_ft_in22k_in1k	88.0	79.76	90.4	90.74	70.68	67.58	57.39	-26
beitv2_large_patch16_224.in1k_ft_in22k_in1k	87.93	79.73	90.16	90.58	70.59	68.16	57.3	-26
caformer_b36.sail_in22k_ft_in1k	87.32	78.34	90.47	90.5	71.3	67.68	57.17	-11
maxxvitv2_rmlp_base_rw_224.sw_in12k_ft_in1k	86.48	76.51	89.81	88.27	68.93	66.53	56.91	+18
beit_large_patch16_384.in22k_ft_in22k_in1k	88.34	80.04	90.62	91.0	70.23	68.32	56.89	-44
caformer_s36.sail_in22k_ft_in1k_384	86.85	78.37	90.36	90.23	71.09	66.61	56.64	+5
maxvit_xlarge_tf_384.in21k_ft_in1k	88.16	79.35	90.2	90.66	70.79	67.25	56.64	-41
maxvit_large_tf_512.in21k_ft_in1k	88.22	79.91	90.4	90.73	72.1	67.77	56.56	-43
convnext_base.clip_laion2b_augreg_ft_in1k_384	86.52	77.17	90.05	88.86	68.72	62.35	56.34	+11
seresnextaa101d_32x8d.sw_in12k_ft_in1k	86.03	76.19	89.65	88.11	68.16	66.36	56.13	+23
eva_giant_patch14_224.clip_ft_in1k	88.92	81.41	91.03	91.92	73.12	67.43	55.91	-59
eva02_base_patch14_448.mim_in22k_ft_in1k	88.03	79.66	90.61	90.89	71.49	66.89	55.81	-38
tf_efficientnet_l2.ns_jft_in1k_475	88.07	80.65	90.56	91.47	70.28	68.61	55.68	-40
convnext_base.clip_laion2b_augreg_ft_in12k_in1k_384	87.12	77.38	90.33	89.83	69.41	64.77	55.58	-14
convnext_large.fb_in22k_ft_in1k	85.76	75.72	89.49	87.69	67.86	66.05	55.56	+20
convnext_large_mlp.clip_laion2b_soup_ft_in12k_in1k_384	88.31	79.47	90.68	90.76	70.01	66.82	55.15	-54
convnext_large_mlp.clip_laion2b_augreg_ft_in1k	87.21	78.26	90.35	89.99	68.82	66.62	54.33	-19
maxvit_large_tf_384.in21k_ft_in1k	87.77	79.19	90.22	90.43	70.98	66.88	53.88	-36
convnextv2_large.fcmae_ft_in22k_in1k	86.42	76.61	89.53	88.19	65.85	64.25	53.87	+4
maxvit_base_tf_512.in21k_ft_in1k	88.14	79.95	90.53	91.11	71.69	68.02	53.69	-52
convnext_large_mlp.clip_laion2b_soup_ft_in12k_in1k_320	87.93	79.03	90.57	90.42	68.11	66.0	53.51	-44
tf_efficientnetv2_m.in1k	84.54	74.06	88.86	86.5	68.27	63.36	53.38	+20
vit_large_patch14_clip_336.openai_ft_in12k_in1k	88.16	80.3	90.45	90.78	68.98	62.5	53.04	-56
caformer_m36.sail_in22k_ft_in1k	86.42	77.53	89.87	89.44	70.17	65.62	52.81	-1
maxvit_base_tf_384.in21k_ft_in1k	87.74	79.33	90.32	90.68	71.24	68.76	51.92	-42
convnextv2_base.fcmae_ft_in22k_in1k	85.72	75.97	89.33	87.85	67.32	65.35	51.88	+10
swin_small_patch4_window7_224.ms_in1k	82.63	70.29	87.42	82.54	64.38	61.95	51.56	+28
coatnet_rmlp_2_rw_224.sw_in12k_ft_in1k	86.34	76.84	89.77	89.02	68.76	64.67	50.89	-2
twins_svt_base.in1k	82.7	70.97	87.41	83.53	63.67	62.71	50.3	+22
vit_large_patch16_384_augreg_in21k_ft_in1k	86.99	77.93	90.1	89.76	69.94	66.93	49.82	-25
coatnet_2_rw_224.sw_in12k_ft_in1k	86.26	76.61	89.79	88.86	69.82	66.98	49.72	-2
beit_large_patch16_224.in22k_ft_in22k_in1k	87.24	78.67	90.1	89.96	68.59	66.77	49.6	-37
twins_pcpvt_large.in1k	82.69	71.34	87.81	83.94	66.06	63.41	49.52	+20
beitv2_base_patch16_224.in1k_ft_in22k_in1k	85.93	76.49	89.65	88.63	68.71	66.26	49.3	+0
xception65.ra3_in1k	82.83	72.02	87.85	84.26	64.9	62.39	48.6	+15

Table 6. Comparing model effectiveness using top-1 accuracy, Real accuracy, and ASMA metrics across ImageNetV1 (V1), ImageNetV2 (V2), and PatchML datasets. Models are ordered by ASMA effectiveness on PatchML, with Δ Rank showing their shift from top-1 V1 ranking.

Checkpoint Name	Top-1 Accuracy		Real Accuracy		ASMA			Δ Rank
	V1	V2	V1	V2	V1	V2	PatchML	
vit_large_patch14_clip_224.openai_ft_in1k	87.61	79.11	90.27	90.26	68.25	64.03	48.44	-51
eca_nfnet_l2.ra3_in1k	84.24	73.78	88.9	86.51	66.97	63.63	47.81	+6
beit_base_patch16_384.in22k_ft_in22k_in1k	86.49	77.14	90.22	89.41	70.35	66.55	47.49	-17
vit_large_patch14_clip_336.laion2b_ft_in12k_in1k	88.13	79.23	90.38	90.68	68.92	65.28	47.04	-70
twins_pcpvt_base.in1k	82.06	70.72	87.53	83.3	65.5	62.7	47.03	+17
deit_base_distilled_patch16_224.fb_in1k	82.64	71.24	87.74	83.68	62.88	59.47	46.74	+13
vit_large_patch14_clip_336.laion2b_ft_in1k	87.79	79.41	90.32	90.67	68.05	63.66	46.65	-61
efficientnetv2_rw_m.agc_in1k	84.09	73.78	88.66	86.45	66.44	64.55	46.55	+1
deit_base_patch16_224.fb_in1k	81.25	69.19	86.18	81.32	63.23	58.27	45.71	+24
vit_large_patch14_clip_224.openai_ft_in12k_in1k	88.11	79.04	90.36	90.78	69.94	65.84	45.34	-75
seresnet152d.ra2_in1k	83.19	72.44	88.04	84.76	65.33	62.31	45.3	+2
vit_huge_patch14_clip_336.laion2b_ft_in12k_in1k	88.53	80.17	90.47	90.92	69.68	65.21	45.15	-89
vit_base_patch16_clip_384.laion2b_ft_in1k	86.56	77.72	90.19	89.88	69.82	65.01	45.07	-30
vit_base_patch16_clip_384.laion2b_ft_in12k_in1k	87.18	78.05	90.17	89.88	66.72	63.96	45.04	-50
tnt_s_patch16_224	80.76	68.77	86.4	81.21	64.0	60.32	45.04	+26
coat_lite_small.in1k	81.53	69.88	86.97	82.19	64.44	62.37	45.0	+10
tf_efficientnetv2_l.in21k_ft_in1k	85.56	75.93	89.34	87.95	67.01	61.83	44.78	-15
visformer_small.in1k	81.35	69.15	86.64	81.54	63.62	58.55	44.71	+13
vit_large_patch14_clip_224.laion2b_ft_in12k_in1k	87.68	78.6	90.29	90.58	68.1	65.13	44.64	-70
resnetv2_50x3_bit.goog_in21k_ft_in1k	83.99	73.15	88.62	85.93	68.92	63.19	44.12	-10
vit_huge_patch14_clip_224.laion2b_ft_in12k_in1k	88.1	79.28	90.36	90.67	68.57	66.61	43.96	-85
resmlp_36_224.fb.distilled.in1k	80.1	68.18	86.12	80.43	61.68	57.85	43.92	+30
convit_small.fb.in1k	80.45	68.77	86.28	81.11	63.05	58.89	43.83	+25
seresnext50_32x4d.racm.in1k	80.51	68.08	86.21	80.53	63.25	57.98	43.59	+21
vit_large_patch14_clip_224.laion2b_ft_in1k	87.07	78.56	90.05	89.86	68.72	64.35	43.49	-59
pit_s_distilled_224.in1k	80.81	68.89	86.56	81.52	63.06	58.14	43.46	+14
levit_384.fb.dist.in1k	81.87	69.32	87.17	81.98	61.78	60.41	42.89	-2
tf_efficientnet_b6.ns.jft.in1k	86.07	76.98	89.67	89.11	67.95	65.79	42.89	-31
pit_s_224.in1k	80.02	67.31	85.65	79.23	60.93	60.16	42.74	+25
vit_base_patch16_clip_384.openai_ft_in12k_in1k	86.89	77.57	90.13	89.74	69.46	65.31	42.66	-57
tf_efficientnet_b7.ns.jft.in1k	86.34	77.69	90.0	89.32	68.27	66.36	42.58	-39
ecaresnet101d.miil.in1k	81.52	69.88	86.75	82.51	62.91	59.36	42.42	-4
vit_huge_patch14_clip_224.laion2b_ft_in1k	87.61	79.24	90.35	90.65	67.85	65.89	42.29	-83
efficientnetv2_rw_s.ra2_in1k	82.57	71.48	87.67	83.93	64.56	61.24	42.23	-13
twins_svt_small.in1k	80.86	68.09	86.4	80.17	62.89	60.09	42.18	+2
twins_pcpvt_small.in1k	80.49	68.24	86.21	80.99	63.19	58.7	42.11	+11
resnext50_32x4d.fb_swsl_ig1b_ft_in1k	81.44	71.25	87.17	83.38	64.56	60.38	41.71	-8
tf_efficientnet_lite4.in1k	81.38	70.39	86.79	83.02	64.21	60.06	40.93	-8
tf_efficientnetv2_xl.in21k_ft_in1k	85.44	75.86	88.75	87.67	64.47	59.44	40.92	-34
deit_small_distilled_patch16_224.fb_in1k	80.11	68.12	86.25	80.31	61.94	58.06	40.81	+11
swin_tiny_patch4_window7_224.ms_in22k_ft_in1k	79.8	68.7	86.47	81.58	63.94	58.54	40.75	+18
regnety_016.tv2_in1k	79.92	68.22	85.89	80.18	63.3	57.36	40.72	+13
ecaresnet50d.miil.in1k	79.73	67.61	85.78	80.12	62.92	58.59	39.45	+17
gernet_l1dstcv_in1k	80.75	68.5	86.17	81.07	63.61	58.69	39.05	-2
ecaresnet50t.ra2_in1k	80.94	69.04	86.54	81.56	63.37	60.23	38.97	-10

Table 7. Comparing model effectiveness using top-1 accuracy, ReaL accuracy, and ASMA metrics across ImageNetV1 (V1), ImageNetV2 (V2), and PatchML datasets. Models are ordered by ASMA effectiveness on PatchML, with Δ Rank showing their shift from top-1 V1 ranking.

Checkpoint Name	Top-1 Accuracy		ReaL Accuracy		ASMA			Δ Rank
	V1	V2	V1	V2	V1	V2	PatchML	
tf_efficientnet_b6.ap_in1k	84.67	74.95	89.38	87.68	68.1	63.1	38.96	-40
deit_small_patch16_224.fb_in1k	78.85	66.19	84.94	78.59	63.04	58.4	38.78	+29
vit_small_r26_s32_384.augreg_in21k_ft_in1k	83.92	73.5	88.81	86.24	68.12	62.33	38.62	-37
pnasnet5large.tf_in1k	82.02	70.67	87.12	82.79	63.24	59.86	38.47	-26
eca_nfnet_l0.ra2_in1k	81.15	69.23	86.92	82.23	64.01	60.47	37.93	-16
resnet50d.a2_in1k	78.93	65.96	84.74	78.4	60.01	55.08	37.71	+23
tf_efficientnet_b5.ns_jft_in1k	85.51	76.27	89.61	88.37	67.77	65.29	37.4	-49
vit_small_patch16_384.augreg_in1k	80.83	69.24	86.23	82.06	64.07	58.56	37.36	-14
coat_mini.in1k	80.61	68.49	86.52	81.35	63.92	61.61	37.02	-10
gmlp_s16_224.ra3_in1k	78.61	66.35	84.47	77.93	62.48	58.13	36.83	+27
csresnext50.ra_in1k	80.15	68.21	85.93	80.19	61.31	57.8	36.77	-6
levit_256.fb_dist_in1k	80.62	67.59	86.16	80.06	59.17	59.36	36.52	-14
hrnet_w18.ms_aug_in1k	77.11	64.84	83.9	77.24	61.05	55.65	36.26	+56
rexnet_200.nav_in1k	80.93	69.07	86.43	81.7	62.5	59.6	36.13	-23
nfnet_l0.ra2_in1k	81.52	69.73	87.01	82.51	64.32	60.05	35.87	-33
seresnet50.ra2_in1k	79.51	66.91	85.42	79.44	62.03	57.13	35.68	+1
tf_efficientnetv2_s.in21k_ft_in1k	82.7	72.3	87.75	84.56	62.93	59.64	35.52	-45
efficientnet_b3.ra2_in1k	80.84	69.36	86.61	81.58	63.41	59.69	35.49	-25
pit_xs_distilled_224.in1k	77.87	65.41	84.48	76.78	58.97	54.7	35.43	+32
ecaresnetlight.miil_in1k	79.2	66.85	85.1	79.24	61.95	56.9	35.28	+3
gernet_m.idstcv_in1k	80.05	67.57	85.77	80.15	60.74	56.78	35.28	-13
resnest50d_4s2x40d.in1k	80.15	68.23	85.75	80.1	61.52	59.58	35.28	-17
resmlp_12_224.fb_distilled.in1k	76.38	63.56	83.41	75.96	59.21	54.07	35.01	+67
resnext50d_32x4d.bt_in1k	78.95	66.28	84.98	78.69	62.6	57.31	34.97	+4
regnety_032.ra_in1k	81.3	69.96	86.89	82.29	65.57	58.06	34.95	-38
inception_resnet_v2.tf_in1k	79.39	67.53	85.44	79.79	61.78	58.15	34.83	-6
pit_xs_224.in1k	76.88	63.99	83.6	75.68	61.1	55.96	34.64	+51
vit_base_patch16_224.augreg_in21k_ft_in1k	83.38	71.91	88.03	84.23	65.42	61.76	34.62	-61
cspdarknet53.ra_in1k	79.33	67.16	85.71	79.67	61.99	56.74	34.58	-7
gmixer_24_224.ra3_in1k	77.17	64.57	83.03	76.34	60.12	56.22	34.54	+38
efficientnet_em.ra2_in1k	78.39	66.29	85.16	78.9	60.67	55.73	34.43	+9
regnety_008_tv.tv2_in1k	77.75	65.07	84.14	77.77	63.0	55.91	34.36	+25
coat_lite_tiny.in1k	75.98	63.23	83.1	75.83	59.46	55.73	34.29	+64
repvgg_b2g4.rvgg_in1k	78.63	66.86	85.15	78.99	60.8	58.62	34.14	+2
resnest50d.in1k	79.82	67.54	85.32	79.99	61.18	57.15	33.92	-22
nf_resnet50.ra2_in1k	79.34	67.36	85.73	79.96	62.42	57.93	33.77	-15
ecaresnet101d_pruned.miil_in1k	79.9	68.02	85.71	80.46	64.26	58.94	33.69	-26
levit_192.fb_dist_in1k	78.78	65.73	84.78	78.3	59.57	57.56	33.68	-6
tf_efficientnet_b4.in1k	81.99	70.14	87.28	82.38	63.7	60.16	33.49	-60
regnetx_004_tv.tv2_in1k	73.83	60.19	81.1	72.47	60.18	52.16	33.05	+86
ecaresnet26t.ra2_in1k	78.04	65.7	84.63	78.1	61.09	56.36	32.31	+2
tf_efficientnet_lite3.in1k	78.95	66.65	85.2	79.05	61.67	56.54	31.56	-15
coat_tiny.in1k	77.45	64.69	84.29	77.28	61.06	56.54	31.15	+16
res2net50_26w_6s.in1k	77.46	64.7	83.86	76.51	59.25	56.27	31.11	+14
rexnet_150.nav_in1k	79.46	67.52	85.65	79.55	62.13	57.38	31.1	-26

Table 8. Comparing model effectiveness using top-1 accuracy, ReaL accuracy, and ASMA metrics across ImageNetV1 (V1), ImageNetV2 (V2), and PatchML datasets. Models are ordered by ASMA effectiveness on PatchML, with Δ Rank showing their shift from top-1 V1 ranking.

Checkpoint Name	Top-1 Accuracy		ReaL Accuracy		ASMA			Δ Rank
	V1	V2	V1	V2	V1	V2	PatchML	
res2net101_26w_4s.in1k	77.98	65.54	84.2	77.97	61.26	55.65	31.05	-1
cspresnet50.ra.in1k	78.75	66.54	85.08	78.9	61.66	56.44	30.93	-14
dla60_res2net.in1k	77.32	64.91	84.24	77.1	62.48	57.03	30.6	+17
res2net50_26w_8s.in1k	77.85	65.77	84.03	78.08	60.68	56.03	30.53	+3
tf_efficientnet_el.in1k	78.88	66.27	85.05	78.27	60.16	54.5	30.3	-20
resnetblur50.bt.in1k	78.04	65.56	84.28	77.81	60.45	57.63	30.29	-9
dla60_res2next.in1k	77.45	65.04	84.03	77.02	60.8	57.56	30.26	+8
resnetrs101.tf.in1k	78.3	66.06	84.16	78.16	58.15	57.75	30.16	-12
dpn68b.ra.in1k	77.35	64.51	83.43	76.47	59.12	53.72	29.83	+8
levit_128.fb_dist.in1k	76.83	63.77	83.46	75.74	58.21	54.74	29.66	+25
resnet34d.ra2.in1k	75.69	63.05	82.89	75.14	59.89	56.29	29.44	+43
res2next50.in1k	76.99	64.05	83.21	76.23	59.9	54.61	29.39	+19
skresnext50_32x4d.ra.in1k	79.19	66.27	84.58	78.11	59.63	55.99	29.17	-34
res2net50_48w_2s.in1k	76.32	63.26	83.06	75.61	61.15	56.56	28.99	+32
tf_efficientnet_b3.aa.in1k	80.23	68.17	85.98	80.31	61.88	58.22	28.93	-56
resnest26d.gluon.in1k	77.01	64.73	83.65	76.61	59.05	55.89	28.85	+13
res2net50_26w_4s.in1k	76.77	63.69	83.41	76.3	60.88	56.3	28.67	+20
convit_tiny.fb.in1k	71.38	58.52	79.31	70.35	57.87	53.48	28.5	+90
vit_small_patch32_384.augreg.in21k_ft.in1k	79.9	68.28	85.93	80.76	63.48	57.68	28.21	-53
ese_vovnet39b.ra.in1k	77.95	65.64	84.58	78.3	61.84	55.62	28.17	-18
legacy_seresnext101_32x4d.in1k	79.16	67.31	84.91	79.37	62.74	57.89	27.7	-41
res2net50_14w_8s.in1k	76.92	63.91	83.28	75.81	61.83	54.5	27.67	+10
vit_small_patch16_224.augreg.in21k_ft.in1k	79.86	67.1	85.54	80.02	63.04	57.39	27.47	-56
dpn92.mx.in1k	77.97	64.88	83.75	77.14	59.04	56.56	27.47	-23
dla102x2.in1k	78.68	66.44	84.62	78.81	60.71	57.24	27.29	-36
tf_efficientnet_b1.ns_jft.in1k	79.62	68.04	85.45	80.52	61.04	57.94	27.09	-55
deit_tiny_distilled_patch16_224.fb.in1k	72.72	59.73	80.25	71.29	54.86	50.5	26.82	+74
hrnet_w40.ms.in1k	77.95	65.09	84.14	77.35	60.77	56.33	26.8	-25
densenetblur121d.ra.in1k	75.13	62.49	82.44	74.27	59.21	52.9	26.6	+36
dpn98.mx.in1k	77.76	64.93	83.79	76.66	60.84	57.57	26.3	-19
dla102.in1k	77.02	64.35	83.5	76.57	61.39	55.81	26.13	-3
dla169.in1k	77.93	65.49	84.18	77.6	62.79	56.15	25.64	-28
seresnext26t_32x4d.bt.in1k	76.83	63.37	83.04	75.91	59.83	54.11	25.58	+3
regnetx_064.pycls.in1k	77.33	64.94	83.43	76.94	60.16	54.92	25.57	-15
pit_ti_distilled_224.in1k	72.51	59.37	79.99	70.98	54.79	52.63	25.31	+68
hrnet_w32.ms.in1k	77.37	64.42	83.74	76.7	61.8	56.62	25.25	-20
vit_small_r26_s32_224.augreg.in21k_ft.in1k	80.5	67.81	85.79	79.74	63.09	58.41	25.24	-81
hrnet_w30.ms.in1k	77.03	64.77	83.59	76.93	60.46	55.47	25.21	-11
regnetx_080.pycls.in1k	77.32	64.06	83.24	76.1	59.31	54.21	25.16	-19
deit_tiny_patch16_224.fb.in1k	69.95	57.05	77.94	68.31	55.4	50.15	25.14	+73
gernet_s.idstcv.in1k	75.66	62.19	82.47	74.37	58.07	52.64	25.11	+16
dla60x.in1k	77.04	64.87	83.61	77.04	61.87	56.93	25.05	-16
resnet50.am.in1k	77.33	63.92	83.71	76.7	60.32	56.31	24.9	-25
seresnext26d_32x4d.bt.in1k	76.64	63.53	82.84	75.35	58.85	55.9	24.75	-5
pit_ti_224.in1k	70.85	57.69	78.52	68.45	56.29	52.62	24.72	+65

Table 9. Comparing model effectiveness using top-1 accuracy, Real accuracy, and ASMA metrics across ImageNetV1 (V1), ImageNetV2 (V2), and PatchML datasets. Models are ordered by ASMA effectiveness on PatchML, with Δ Rank showing their shift from top-1 V1 ranking.

Checkpoint Name	Top-1 Accuracy		Real Accuracy		ASMA			Δ Rank
	V1	V2	V1	V2	V1	V2	PatchML	
efficientnet_b2.ra.in1k	78.97	65.92	84.95	77.96	60.12	55.99	24.69	-65
legacy_seresnext50_32x4d.in1k	77.93	65.45	84.08	77.81	61.06	54.26	24.68	-42
nf_regnet_b1.ra2.in1k	77.85	65.37	84.34	77.83	60.53	58.79	24.59	-40
mixer_b16_224.goog.in21k_ft.in1k	73.94	59.21	79.52	70.27	52.67	46.31	24.55	+30
regnetx_040.pycls.in1k	76.87	63.2	83.09	75.3	58.13	54.72	24.53	-16
resnet26d.bt.in1k	75.25	61.44	81.76	73.67	58.06	55.13	24.49	+11
mobilenetv2_120d.ra.in1k	76.04	62.89	82.9	74.82	58.57	52.67	24.24	-1
mixnet_xl.ra.in1k	79.5	66.91	85.11	78.97	62.24	57.26	24.0	-80
tf_efficientnet_lite2.in1k	75.67	62.06	82.47	73.96	58.16	55.15	23.94	+2
ese_vovnet19b_dw.ra.in1k	75.44	61.56	82.2	73.3	57.76	52.58	23.87	+4
rexnet_130.nav.in1k	78.51	65.62	84.7	77.54	61.58	56.28	23.87	-62
tf_efficientnetv2_b3.in1k	78.63	66.02	84.52	78.37	60.27	57.46	23.82	-67
tf_efficientnet_cc_b1_8e.in1k	77.07	63.86	83.21	76.0	57.58	57.25	23.76	-33
efficientnet_b2_pruned.in1k	78.59	66.5	84.6	78.47	61.1	56.13	23.68	-66
regnety_040.pycls.in1k	77.81	64.59	83.73	76.55	59.36	55.94	23.56	-51
densenet121.ra.in1k	73.59	60.86	81.11	73.0	56.57	52.83	23.3	+25
regnetx_032.pycls.in1k	76.18	63.21	82.46	75.53	59.26	54.75	22.95	-14
repvgg_b1.rvgg.in1k	77.24	64.96	83.34	76.86	58.54	54.87	22.75	-42
densenet161.tv.in1k	75.25	62.13	82.07	74.16	57.58	53.87	22.71	-3
legacy_seresnet50.in1k	76.26	63.13	82.6	75.1	60.36	55.37	22.66	-18
tf_efficientnet_em.in1k	75.77	62.51	82.42	74.25	57.16	53.25	22.58	-13
tf_efficientnet_b2.in1k	77.24	63.8	83.48	75.76	57.86	55.53	22.57	-45
efficientnet_es_pruned.in1k	73.34	60.43	80.96	72.45	56.32	51.81	22.2	+26
resnet26.bt.in1k	73.61	60.02	80.55	71.86	56.32	51.64	22.11	+16
vit_tiny_patch16_384.augreg.in21k_ft.in1k	78.01	65.95	84.38	77.9	63.29	55.53	21.94	-71
densenet201.tv.in1k	74.56	61.77	81.3	73.59	57.35	52.8	21.9	+2
densenet169.tv.in1k	73.75	59.88	80.69	71.72	54.85	51.8	21.8	+10
mixnet_l.ft.in1k	77.8	64.67	83.93	76.35	59.47	54.48	21.8	-63
tf_efficientnet_lite1.in1k	74.28	61.06	80.97	72.85	56.56	52.95	21.49	+3
resnest14d.gluon.in1k	73.27	59.73	80.32	71.61	56.03	52.22	21.23	+21
mobilenetv2_140.ra.in1k	74.9	61.08	81.77	73.17	56.56	51.83	21.22	-8
resnetrs50.tf.in1k	74.76	60.79	81.04	72.54	56.37	52.46	20.99	-7
skresnet34.ra.in1k	75.06	62.31	82.04	74.07	59.34	52.12	20.68	-12
tf_mixnet_l.in1k	76.63	63.51	82.84	75.08	57.35	53.48	20.67	-39
efficientnet_b1.ft.in1k	76.39	63.54	82.6	75.15	57.34	52.39	20.49	-36
efficientnet_b0.ra.in1k	76.09	62.9	82.67	74.66	59.12	53.32	20.32	-31
regnetx_016.pycls.in1k	74.91	61.14	81.31	72.87	57.33	53.73	20.3	-15
repvgg_a2.rvgg.in1k	75.31	62.55	81.98	73.76	56.98	51.72	20.29	-23
mobilenetv2_110d.ra.in1k	73.34	60.18	80.53	71.73	56.52	51.78	20.28	+9
rexnet_100.nav.in1k	77.0	63.67	83.4	75.66	59.39	54.3	20.25	-55
tf_efficientnet_es.in1k	73.75	60.37	80.52	71.77	54.75	49.79	20.22	-3
tf_efficientnetv2_b2.in1k	76.49	63.42	82.84	75.07	57.66	54.38	20.21	-45
tf_efficientnet_cc_b0_8e.in1k	75.23	61.82	81.85	73.61	56.72	54.26	20.03	-25
fbnetc_100.rmsp.in1k	73.47	59.59	79.93	70.96	54.67	51.52	19.99	-1
mixnet_m.ft.in1k	75.69	62.6	82.09	74.18	57.84	53.77	19.64	-35

Table 10. Comparing model effectiveness using top-1 accuracy, ReaL accuracy, and ASMA metrics across ImageNetV1 (V1), ImageNetV2 (V2), and PatchML datasets. Models are ordered by ASMA effectiveness on PatchML, with Δ Rank showing their shift from top-1 V1 ranking.

Checkpoint Name	Top-1 Accuracy		ReaL Accuracy		ASMA			Δ Rank
	V1	V2	V1	V2	V1	V2	PatchML	
tf_efficientnet_b0.aa.in1k	74.27	60.77	81.12	72.27	57.04	53.84	19.55	-13
dla34.in1k	73.19	60.38	80.36	71.89	57.01	53.91	19.35	+5
efficientnet_lite0.ra.in1k	73.54	59.87	80.6	71.4	56.06	51.04	19.28	-6
hardcorenas_f.miil.green.in1k	76.65	63.72	83.1	75.41	58.26	52.3	19.26	-56
hardcorenas_e.miil.green.in1k	76.51	63.29	82.81	75.09	57.54	51.65	18.96	-54
mnasnet_100.rmisp.in1k	72.6	58.79	79.72	70.43	54.73	50.32	18.94	+6
mobilenetv3_rw.rmisp.in1k	73.92	59.78	80.64	71.65	56.93	49.97	18.65	-17
mixnet_s.ft.in1k	74.33	61.05	81.0	72.46	57.53	52.26	18.48	-22
tf_efficientnet_cc_b0_4e.in1k	74.47	60.53	81.02	72.09	55.69	53.86	18.4	-24
tf_efficientnetv2_b1.in1k	74.64	61.06	81.18	72.57	56.2	52.31	18.27	-29
spnasnet_100.rmisp.in1k	72.47	58.4	79.17	69.33	54.84	50.68	18.19	+3
tf_mixnet_m.in1k	74.58	61.01	81.02	72.6	56.97	53.47	18.11	-30
vit_tiny_r_s16_p8_384.augreg_in21k_ft.in1k	75.18	62.74	82.17	74.99	61.4	53.75	18.09	-39
hardcorenas_d.miil.green.in1k	76.17	62.51	82.45	74.13	56.35	51.02	17.95	-55
regnety_006.pycls.in1k	73.03	58.8	79.53	70.11	55.62	51.39	17.61	-6
tf_efficientnetv2_b0.in1k	73.42	59.95	80.04	71.5	55.01	52.06	17.45	-17
tf_efficientnet_lite0.in1k	71.71	57.65	78.85	68.94	53.12	50.62	17.37	+0
regnetx_008.pycls.in1k	72.09	58.0	78.83	69.56	54.02	52.68	17.34	-3
mobilenetv2_100.ra.in1k	70.81	56.87	78.13	68.25	53.42	49.34	17.33	+2
mobilenetv3_large_100.miil.in21k_ft.in1k	76.44	63.12	82.46	74.89	57.4	51.91	17.3	-67
semnasnet_100.rmisp.in1k	73.41	59.93	80.38	71.76	57.04	51.27	17.24	-21
hardcorenas_c.miil.green.in1k	75.58	61.87	81.97	73.6	58.45	52.07	17.16	-54
legacy_seresnet34.in1k	73.32	59.63	80.12	71.55	56.96	52.54	17.01	-18
repvgg_b0.rvvg.in1k	73.61	60.53	80.37	71.78	56.56	51.17	16.81	-30
skresnet18.ra.in1k	70.71	57.26	78.33	68.91	54.93	50.54	16.78	-3
vit_small_patch32_224.augreg_in21k_ft.in1k	73.39	59.74	80.01	71.73	56.54	53.34	16.6	-25
tf_mixnet_s.in1k	73.37	59.27	79.95	70.75	55.87	52.96	16.56	-25
hardcorenas_b.miil.green.in1k	74.77	60.9	81.28	72.56	57.65	50.99	16.35	-49
hardcorenas_a.miil.green.in1k	74.52	59.99	80.89	71.77	56.68	50.56	16.32	-45
regnetx_006.pycls.in1k	70.97	57.39	77.76	68.32	53.76	50.64	15.83	-11
vgg13_bn.tv.in1k	69.79	56.88	77.27	68.23	54.16	50.9	15.41	-7
vit_tiny_patch16_224.augreg_in21k_ft.in1k	72.95	59.75	79.76	71.27	56.06	50.81	15.37	-22
legacy_seresnet18.in1k	69.12	55.37	76.58	66.59	53.04	50.07	14.58	-7
vgg11_bn.tv.in1k	68.63	54.5	76.02	65.77	54.58	49.46	14.31	-6
tf_mobilenetv3_large_100.in1k	73.09	58.58	79.66	69.71	55.3	51.55	13.65	-27
ghostnet_100.in1k	72.0	57.93	78.82	69.08	54.53	48.94	13.63	-20
dla46x_c.in1k	63.82	50.13	71.34	60.86	49.0	44.78	13.32	-5
dla46_c.in1k	62.41	48.58	69.94	58.57	48.13	45.36	12.45	-5
tf_mobilenetv3_large_minimal_100.in1k	69.14	54.51	75.88	65.79	51.04	49.2	12.13	-14
tf_mobilenetv3_large_075.in1k	70.85	56.41	77.55	67.66	53.36	50.6	11.9	-20
resnet18.gluon.in1k	67.51	53.84	74.65	64.45	52.27	49.3	11.86	-12
vit_tiny_r_s16_p8_224.augreg_in21k_ft.in1k	68.67	54.46	75.74	65.41	52.66	48.5	11.21	-15
regnetx_002.pycls.in1k	65.01	50.7	72.04	60.69	49.35	45.52	10.99	-13
tf_mobilenetv3_small_100.in1k	63.83	49.73	70.43	59.91	48.55	44.43	7.09	-13
tf_mobilenetv3_small_075.in1k	61.44	47.4	68.16	57.34	45.36	44.58	6.81	-11